SATELLITE OBSERVATIONS AND NUMERICAL SIMULATIONS OF JET-FRONT GRAVITY WAVES OVER NORTH AMERICA AND NORTH ATLANTIC OCEAN

A Thesis

by

MENG ZHANG

Submitted to the Office of Graduate Studies of
Texas A&M University
in partial fulfillment of the requirements for the degree of

MASTER OF SCIENCE

August 2008

Major Subject: Atmospheric Sciences

SATELLITE OBSERVATIONS AND NUMERICAL SIMULATIONS OF JET-FRONT GRAVITY WAVES OVER NORTH AMERICA AND NORTH ATLANTIC OCEAN

A Thesis

by

MENG ZHANG

Submitted to the Office of Graduate Studies of
Texas A&M University
in partial fulfillment of the requirements for the degree of

MASTER OF SCIENCE

Approved by:

Chair of Committee,	Fuqing Zhang
Committee Members,	Kenneth Bowman
	Craig Epifanio
	Jiaunghua Huang
Head of Department,	Kenneth Bowman

August 2008

Major Subject: Atmospheric Sciences

ABSTRACT

Satellite Observations and Numerical Simulations of Jet-front Gravity Waves over North America and North Atlantic Ocean.

(August 2008)

Meng Zhang, B.S.; M.S., Nanjing University

Chair of Advisory Committee: Dr. Fuqing Zhang

In this study, a month-long simulation of gravity waves over North America and North Atlantic Ocean is performed using the mesoscale model MM5 for January 2003, verified with Advanced Microwave Sounding Unit-A (AMSU-A) radiance observations in the upper troposphere and lower stratosphere. According to the monthly mean statistics, four regions of strong gravity wave activities are found both in the simulation and the AMSU-A observations: northwestern Atlantic, Appalachian Mountains, Rocky Mountains and Greenland, respectively. Those over the northwestern Atlantic Ocean are strongly associated with the midlatitude baroclinic jet-front systems, while the other three regions are apparently collocated with high topography.

Imbalance diagnosis and numerical sensitivity experiments of a strong gravity wave event during January 18-22 show that the gravity waves are strongly linked to the unbalanced flow in the baroclinic jet-front system. The gravity waves are usually radiated from the upper tropospheric jet exit region with maximum nonlinear balance equation residual (ΔNBE; key indicator of flow imbalance), distinctly different from

other surface sources. Flow imbalance related strongly to tropopause folding and frontogenesis of the large-scale background flow. Similar wave characteristics are simulated in experiments with different microphysics and grid resolutions. The ΔNBE is again shown to be a good predictor for jet-front related gravity waves, suggesting its potential application to gravity wave parameterizations for global and climate models.

ACKNOWLEDGEMENTS

I would like to thank my committee chair, Dr. Fuqing Zhang, for his guidance and support throughout the course of this research, and my committee members, Dr. Kenneth Bowman, Dr. Craig Epifanio, and Dr. Jianhua Huang for their expertise.

Thanks also go to my friends and colleagues, Shuaguang Wang, Ellie Meng, Yonghui Weng, Matthew Rigney, Jason Sippel, Tingting Qian and Juan Fang, and the department faculty and staff for making my time at Texas A&M University a great experience. Special thanks to Shuguang for his insightful discussions and help on experimental implementation.

Finally, I deeply thank my mother and father for their encouragement, and to my girlfriend, Liyun, for her patience and love.

The research is supported by the NSF Grants ATM-0203238 and ATM-0618662.

TABLE OF CONTENTS

Page

ABSTRACT iii

ACKNOWLEDGEMENTS v

TABLE OF CONTENTS vi

LIST OF FIGURES vii

1. INTRODUCTION 1

2. METHODOLOGY 7

    2.1 Modeling gravity waves 7
    2.2 AMUS-A observations 9
    2.3 Case study for a strong jet-front gravity wave event 10

3. MORPHOLOGY OF GRAVITY WAVES OVER NORTH AMERICA AND NORTH ATLANTIC DURING THE MONTH OF JANUARY 2003 12

4. SENSITIVITY STUDY ON A STRONG JET-FRONT GRAVITY WAVE EVENT 20

    4.1 Control simulation of jet-front gravity wave generation 20
    4.2 Sensitivity experiments 28

5. SUMMARY AND DISCUSSIONS 38

REFERENCES 43

APPENDIX A 48

VITA 52

LIST OF FIGURES

FIGURE Page

1 Monthly mean perturbation kinetic energy (a) at 21 km, in unit of $m^2 s^{-2}$, with jet stream (dashed line) and pressure (solid line) at 12 km; and monthly AMSU-A radiance variance (b) at channel 10, in unit of K^2, with mean background flows at 300 mb. The contours of jet are at 45, 55, 65 m/s. 13

2 Monthly mean zonal (shaded) and meridinol (contour, positive in red and negative in blue, with interval of 4) momentum fluxes at 21 km, , in unit of $x10^{-2} m^2 s^{-2}$ 15

3 Monthly mean background flows, including: pressure (black thick) and jet (orange solid, at 35, 45, 55 m/s) at 12 km, bulk vertical shear (dashed green line, at 3.5, 4.0, 4.5 $m s^{-1} km^{-1}$) between 2 and 12 km and reflectivity at 1.5 km 18

4 Gravity waves derived from CNTL at (a) 06Z (b) 12Z (c) 18Z (d) 00Z 19~ 20 January 2003, including 18-km horizontal divergence (negative in red; positive in blue) at 18 km, with intervals of ± 5 ± 15 ± 25 x $10^{-5} s^{-1}$, 12-km pressure (solid line, unit in mb) and jet stream (shaded, unit in $m s^{-1}$) shown at 12 km 21

5 Channel 9 (18-km equivalent) AMSU-A radiance perturbation (shaded, unit in K) shown at (a) 06Z (b) 12Z (c) 18Z (d) 00Z 19~20 January 2003 . 22

6 CNTL horizontal (left column, at 15 km) and vertical (right column) structures of incipient jet-front gravity waves, (a) (b) for 00Z, (c) (d) for 06Z and (e) (f) for 12Z, 19 January 2003: including vertical velocity (positive in red, negative in blue) shown at ± 0.05 ± 0.15 ± 0.25 $m s^{-1}$, 12-km jet stream (shaded, unit in $m s^{-1}$) and pressure (solid black, unit in mb), reflectivity (yellow) with 20 dBZ interval, large-scale NBE residual (thick green) with 2 x $10^{-9} s^{-2}$ interval and potential temperature (gray line) with 10 K interval upper 320 K and 4 K interval below. The position of cross section is marked as dashed line 25

7 Same as Fig. 6, but for mature stage: (a) (b) for 18Z 19 January 2003, (c) (d) for 00Z 20 January 2003. 26

8 30DRY experiment at 00Z (a) (b), 12Z (c) (d) 19 January and 00Z (e) (f)

FIGURE Page

20 January 2003: the legends are the same as Fig. 6. Additional line of NBE residual added at 1 x 10^{-9} s^{-2} (dashed green line) 30

9 Same as in Fig. 8 but for *10KM* experiment and without large-scale NBE residual 31

10 Same as in Fig. 8 but for *10DRY* experiment and without large-scale NBE residual 32

11 The *120KM* experiment at 00Z (a) (b), 12Z (c) (d) 19 January and 00Z (e) (f) 20 January 2003: horizontal (left column, 8 km) and vertical (right column) NBE residual (green line) with 2 x 10^{-9} s^{-2} interval, Miller frontogenesis function (red line) shown in vertical with 0.2 K (100 km h)$^{-1}$ interval, and dynamical tropopause (thick black) labeled at 1.5 PVU. 8-km jet stream (shaded) and potential temperature are labeled as same in Fig. 6..... 34

12 18-km zonal (shaded) and meridional (positive in red, negative in blue) momentum flux of jet-front GW (left column) and convection-GW (right column) in CNTL, shown at (a) (b) 12Z January 19 and (c) (d) 00Z January 20 2003. The intervals are 30 m^2 s^{-2} for left column, and 10 m^2 s^{-2} for right column..... 36

13 Flight-based measurements and numerical simulations from START08: (a) 15-km forecast valid at 22Z 21 April 2008, for 12-km (around flight height) vertical velocity (positive in red, negative in blue, with 0.03 m s^{-1} interval), 9-km pressure (solid, unit in mb) and jet (shaded, with 10 m s^{-1} interval), flight track marked as AB and AC (thick green line); flight-observed potential temperature (K), for AB (b) and AC (c) during reference time..... 42

14 Flowchart of the real-time assimilation/forecast system for START08 44

15 The RMS errors of EnKF prior (solid blue) and posterior analysis (solid red) against radiosonde observations, valid at 12Z 21 April 2008, for zonal wind (a), meridional wind (b), temperature (c) and mixing ratio (d). And predicted RMS error (RMS error plus observational error) (dashed dot) and ensemble spread (dot) are also shown for them..... 45

1. INTRODUCTION

Gravity waves (GWs) are one of the most important dynamical processes in the atmosphere, whose generation and propagation could impact general circulations, especially for the energy and momentum exchanges between troposphere and stratosphere. Typically, mesoscale GWs have horizontal wavelength of 50-500 km, with 1-15 hPa surface amplitude and intrinsic period about 0.5-4 h. However, due to their shorter wavelength and period comparing to the other synoptic waves, they are relatively hard to be captured by conventional observations, and also not easily to be simulated explicitly in numerical weather prediction models (Hamilton 1996, Kim et al. 2003).

There are several mechanisms for GW generation, such as convection, shear instability, topography, frontogenesis and geostrophic/imbalance adjustments (Fritts and Alexander 2003), where the last one is the main concern for this study. It has been documented that midlatitude geostrophic imbalance could radiate gravity waves spontaneously, where the most favorite region for such waves is over the vicinity of an unbalanced jet streak in the upper troposphere (Uccellini and Kocj 1987). The region usually could be bounded by jet streak, surface front, inflection axis and the 300hPa ridge line (refer to Fig. 2, Koch and Handley 1997). Numerical simulations also suggested the continuous GW generations from imbalance adjustment. O'Sullivan and Dunkerton (1995) used a three-dimensional nonlinear model to demonstrate that inertia-gravity wave may arise as the tropospheric jet stream is distorted by baroclinic instability and strong parcel accelerations take place, primarily in the vicinity area of the upper tropospheric jet

---

This thesis follows the style of *Monthly Weather Review.*

stream. However, due to the limitation of model resolution, most of the subsynoptic-scale GW (as 50-500km) features could not be captured in their study.

More comprehensive works based on various observations, such as surface observations, radiosondes, radar and satellite, are given out by Bosart et al. (1998) to provide us some general images for such GW generation for a strong gravity wave event. But similar to those simulated by coarse-resolution models, the GWs with mesoscale nature are not easily captured by current observational network either. Case studies via conventional observations would suffer from limited data both temporally and spatially. Intensive field observations and high-resolution measurements are desired for GW diagnostics. For instance, high vertical resolution radiosonde could provide us more decent observations for the climatology of GW activities, and also separate the GW sources and propagations at different levels with various horizontal maxima (Wang and Geller 2003; Wang et al. 2005). Similar work was also found in Plougonven et al. (2003), where intensive ship-based radio soundings over North Atlantic storm-track regions were obtained to reveal the jet-front GW generations. And GPS OS (occultation sounding) is more powerful on such studies owing to its significant coverage over oceans and very high-resolution vertical profiles (refer to GPS/MET and GPS/CHAMP, Tsuda et al. 2000; Ratnam et al. 2004).

On the other hand, even in the cases with observed GW activities, it is usually very difficult to distinguish waves generated by various mechanisms. E.g., in the jet-front system, imbalance adjustment, convections and surface front are all of the possible sources for mesoscale GWs. Fritts and Nastrom (1992a,b) used aircraft measurements to investigate the different sources of GW as jet streaks (convections, front and topography,

respectively), and found that mesoscale variances of horizontal wind and temperature were large at the jet-front vicinity regions. Based on a 3-year statistical analysis of MU radar data, Sato (1994) also gave out a good correlation between jet strength and GW signals along with their seasonal variability. More recently, Nastrom and Eaton (2006) and Vaughan and Worthington (2007) assessed MST radar data over several years to examine the GWs in both the stratosphere and the troposphere, which also revealed substantial association of GWs with jet streaks.

More sophisticated high-resolution simulations of jet-front GWs through a complex mesoscale model were presented by Zhang et al. (2001, 2003) on a large-amplitude GW event along the east coast of U.S., where wavelet, spectral and imbalance analyses were used to reveal the multi-scale interactions of wave generations: the upstream increasing imbalance associated with upper-level troposphere folding immediately radiate the GWs several hours before its surface sources; a new conceptual model showed the different stages of jet-front GW evolution and its interaction with jet streams. Higher resolution, down to 3.3km, is applicable to reproduce those observed GWs with horizontal wavelength about 100-200 km in an idealized case, which are excited from the exit region of an upper-tropospheric jet streak (Zhang 2004). This idealized work within a pure baroclinic jet-front environment clearly demonstrated that, through balance adjustment, the continuous generation of imbalance from a developing baroclinic wave system results in the spontaneous emissions of mesocale GWs. Further studies of such idealized pattern are conducted by Lin and Zhang (2008), which are addressed to investigate the propagating characteristics and possible source mechanisms of jet-related GWs through 2-D Fourier decomposition and ray-tracing techniques: four

groups of GW are found with different wavelength and generation/propagation features, for such medium-scale GWs with 350-km wavelength are clearly orientated from upper-troposphere jet-front system with maximum imbalance. And the wave characters of jet-front GW are associated with its baroclinic background: higher growth rate of baroclinicity could generate higher flow imbalance increasing, and then impact the intrinsic frequency of GW (Wang and Zhang 2007). Another similar work by Plougonven and Snyder (2007) claimed that the sources of jet-front GW excitations strongly depend on the details of the baroclinic wave's development, where more jet-GWs are generated from a cyclonic type of baroclinic instability and front-GWs are generated from anticyclonic one. The same studies of GW sourced from frontogenesis are also found in Snyder et al. (1993) and Griffiths and Reeder (1996), and the tentative parameterization of such type of GW in global model was firstly demonstrated by Charron and Manzini (2002).

Moreover, jet-front GW generated by spontaneous emission mechanism is also simulated in another setup of jet streak within an idealized vortex-dipole (Snyder et al. 2007). Because of the persistent radiations of mesoscale GWs in the dipole system, it can be proved as an inherent feature of such localized jet flows and associated with the imbalance adjustment. Based on the ray-tracing analysis of those phased-lock GWs against jet streams, their wave characteristics are strongly related to the jet strength in this dipole system (Wang et al. 2008).

With limited in-situ observations, various remote sensing measurements from NOAA satellites provide valuable information about the characteristics and distribution of gravity waves over upper troposphere and lower stratosphere (UTLS) regions,

especially for the mountain and ocean areas, where ground-based measurements are sparse or not available. The microwave sounders have been proven to be utilized for GW detections, e.g., MLS and AMSU-A. Their applicable resolution and well coverage could map those GW activities through the radiance variances, which imply the temperature perturbations that derived by GW over UTLS. And their profiles also could be used to retrieval the GW propagation in vertical direction. Wu and Waters (1996) found that the MLS oxygen radiance is sensitive to GW perturbations of short (<100 km) horizontal and large (>10-km) vertical wavelength. More details of GW analysis with MLS were given by Jiang et al. (2004) for Northern Hemisphere winter, where plenty topographic GWs are identified over those significant mountain areas, such as Alaska, Canada, Greenland, Scandinavia and Russia. Meanwhile, Wu and Zhang (2004) investigated the applications of AMSU-A data for jet-front GW diagnostics, the products of which has higher resolution and longer records. And the data from different channels are used to project the GW vertical features. Even though those new techniques give us more evidences and direct images for GW activities, however, there is still lack of understanding for the generation and maintenance mechanisms of those mesoscale waves, where more comprehensive studies both on modeling and observation verifications should be considered.

In this study, following Wu and Zhang (2004) and Zhang et al. (2001, 2003 and 2004), a month-long simulation via the MM5 model will be conducted to examine GW generations and propagations over North America and North Atlantic Ocean in a winter season, when westerly upper-level jet streaks are stronger than the other seasons. Based on the climatological statistics of the model results, we try to find out the favorite GW

regions over North America and North Atlantic Ocean, and subsequently verify the model results with AMSU-A observations. Considering the jet-front system is one of the most important sources for GW generation and the key part of this study, a case study will be produced to investigate such mechanism with both dynamical details and sensitivity test. Through clarifying jet-front GW from the other sources, a possible method that estimates GW momentum contributions for large-scale flows will be discussed based on such case study.

Experiment design and diagnostic methods are presented in the next section. And the morphology of GW activities over North America and North Atlantic Ocean during a winter month is given in Section 3. Sensitivity tests of jet-front GW generation are provided in Section 4 based on a strong GW event over northwestern Atlantic. Summary and conclusions are placed in Section 5.

2. METHODOLOGY

To archive the research purpose of this work, there are mainly three steps of the methodology: 1) modeling and diagnostics of GW activities for the month of January 2003; 2) verification of model simulations against AMSU-A satellite measurements; 3) case study and sensitivity test on jet-front GW generations of a strong gravity wave event during 18-22 January 2003. More specifications of each part are listed in following:

2.1 Modeling gravity waves

The PSU-NCAR mesoscale model MM5 (Grell *et al.* 1994) is used to investigate the GW activities over North America and North Atlantic Ocean regions. MM5 is a non-hydrostatic model with terrain-following vertical sigma coordinate, which has the capability to simulate both the generation and propagation of gravity waves with various sources (Zhang et al. 2001, Zhang 2004).

For the control simulation, a single domain with 300 x 200 grid points and 30-km horizontal resolution is employed to cover the whole North America and North Atlantic Ocean, which includes 90 vertical levels up to 10 mb (about 25-km height). To keep the background flow of model simulation from drifting too far away from the truth state, there are totally 12 separated but sequential simulations, each with a 72-h integration, to cover the whole month, where the initial and lateral boundary conditions for each simulation are interpolated from the European Center for Medium-Range Weather Forecasts (ECMWF) daily analysis with 2.5 x 2.5 degree resolution. A 12-h spin-up time

is needed for each simulation, thus a 12-h overlap is placed between every two adjacent runs.

The Grell cumulus parameterization scheme (Grell *et al*. 1993), mixed-phase microphysics scheme (Reisner *et al*. 1998) and medium-range forecast (MRF) planetary boundary layer (PBL) parameterization scheme (Hong and Pan 1996) are employed for all numerical runs (as in Wu and Zhang 2004). The background flows of each 72-h simulation are verified against the daily ECMWF analysis, which indicate that the main patterns and strength of upper-level jet streaks still keep their main features all through the month-long integrations (not shown).

In previous works, GW signals could be diagnosed by divergence and vertical velocity fields at upper levels (300 hPa or higher), as in case studies of Zhang et al. (2001, 2003). Since here we focus on the short-term climatology of the gravity wave activity, the perturbation energy and momentum flux are used, with the same as in Sato et al. (1999):

$$KE = \frac{1}{2}(\overline{u'^2} + \overline{v'^2} + \overline{w'^2}) \tag{1}$$

$$PE = \frac{1}{2}(\frac{g^2}{N^2})(\frac{\overline{\theta'^2}}{\overline{\theta}^2}) \tag{2}$$

Where *KE* and *PE* are the kinetic and potential energy per unit mass of GW perturbations, *u'*, *v'*, *w'* and θ' are the perturbation components of zonal, meridional, vertical winds and potential temperature; *N* is the Brunt-Vaisala frequency. In fact, the ratio of KE/PE is nearly a constant if the main characteristics (e.g., wavelength) of GW do not change significantly (Gill 1982, page 255), so that only *KE* is used in this study to

diagnose GW activities. A band-pass filter will be applied to extract GW perturbations with wavelength from 200 to 600 km, and then calculate the monthly averaged GW kinetic energy by formula (1), where the same cut-off wavelength is used for all variables (u, v and w). Then monthly mean distribution of GW activities could be obtained. And the structure of the vertical flux of horizontal momentum (i.e., momentum flux) produced by GW could reach the stratosphere and mesosphere, and then impact their main circulations, thermal structures and species distribution, especially for those radiation-sensitive variables. Therefore, the GW momentum flux maps could be useful for us to understand the GW contributions over North America and North Atlantic Ocean regions, where zonal and meridional momentum fluxes are defined as, $\overline{u'w'}$ and $\overline{v'w'}$, respectively.

2.2 AMUS-A observations

Three similar AMUS-A measurements operated by National Oceanic and Atmospheric Administration (NOAA) are used to verify model results, i.e., NOAA 15, NOAA 16 and NOAA 17. Each satellite can provide two observations in every day, hence totally 6 observations are available with about 4-h intervals, and such time period varies with daily orbits. The scan swath of those NOAA satellites is about 2300 km with few gaps between the orbits, where the horizontal resolution is about 50~110 km, about 90 km in average (Wu 2004).

There are 15 sounding channels of AMSU-A instruments, six of which (channel 9~14) have the peak temperature weighting functions at 18, 21, 26, 33, 38 and 45 km height, respectively, covering upper troposphere and stratosphere over mid-latitude

regions. Channels of 1-8 and 15 are not used in this study because larger impacts from surface emission and cloud scattering would affect the accuracy of AMSU measurements. The GW perturbations could be detected by the AMSU radiance maps, and consequently their monthly variances could reveal the main favorite GW regions. The data processing and quality control of AMSU-A observations are conducted based on the methods in Wu and Zhang (2004), where the background radiance is carefully taken off by a 2-D nine-point running window to treat the large-scale signals (> 600 km).

2.3 Case study for a strong jet-front gravity wave event

Based on the numerical results and their statistics, sensitivity experiments are performed for a selected strong GW event during 18-22 January 2003, over northwestern Atlantic, as an extension of Wu and Zhang (2004). For one thing, detailed GW generation/propagation characteristics and associated background flow features, including both GW and imbalance diagnostics, will be addressed to investigate the jet-front GW generation mechanism in a real case, following those idealized works, so that the incipient stage of GW generation is our major concern. For another, the numerical sensitivity will be tested under various model configurations: 1) the comparison between moist and fake-dry runs could provide a better view to clarify jet-front GW sources from excluding the GWs that induced by convections; 2) tests with different model resolutions, e.g., from 30 km down to 10 km or up to 120 km, could also be applied to test the representativity of those model simulations, whether or not sub-scale problems are crucial for different runs, such issue is related to the credibility of model results and their application prospect in the parameterization of jet-front GWs in coarse runs (120 km for

this case and also applicable for other global models), which needs a reliable and consistent estimation on their wave characteristics and momentum contributions.

For the studies on jet-front GW generation, the methods to diagnose their origins (i.e., unbalance flow) are also important, where imbalance adjustment is regarded as a key factor for jet-front GW generations and the main concern in this study. In practical, there are several paths for imbalance flow detection, such as Rossby number (Koch and Dorian 1988), Psi vector (Longhe et al. 1995), omega equations (Krishnamurti 1968), PV inversion (Davis and Emanuel 1991) and nonlinear balance equation residual (Zhang et al. 2001), where the NBE residual (ΔNBE) is suggested as a very effective sign for imbalance occurrence, and then it is promising to implement it as a precursor to predict GW generation (Zhang 2004). The ΔNBE is expressed as:

$$\Delta NBE = 2J(u,v) + f\zeta - \nabla^2\Phi - \beta u \qquad (3)$$

where J is the Jacobian term, $\beta = \partial f / \partial y$, Φ is the geopotential height and ζ is the relative vorticity, respectively. The more recent work of Plougonven and Zhang (2007) demonstrated the NBE residual forcing on spontaneous GW generations through the scale analysis of primitive equations. However, the problem is that GW itself are also contribute to NBE imbalance, so that it will be hard to discriminate the unbalance flow and GW signals when GWs are generated continuously, especially in real-case experiments. In this study, we use a low-pass filter with cut-off of 900 km to extract large-scale NBE residuals that simply driven by synoptic dynamical systems, and its patterns could be verified by coarse runs (i.e., 120 km run).

3. MORPHOLOGY OF GRAVITY WAVES OVER NORTH AMERICA AND NORTH ATLANTIC OCEAN DURING THE MONTH OF JANUARY 2003

Using the monthly-long high-resolution simulations over North America and North Atlantic, we can estimate the main features of GW morphology in the middle and higher latitudes. Since the GW intensity is consistently stronger in winter than other seasons, both in previous observational and modeling studies (e.g., Sato et al. 1999, Wang and Geller 2003), we choose a typical winter month, January 2003, in this case, which is also regarded as a strong GW year in last decade based on the statistical analysis of AMSU-A data (Wu and Zhang 2004).

The perturbation kinetic energy (see to Section 2.1) is calculated at every 3 hours and averaged over the month period, which is used to estimate the GW activities. Its distribution in stratosphere (21-km height), along with major atmospheric circulations (12-km height, jet-core level), is shown in Fig. 1a, where several active GW areas are found over North America and North Atlantic Ocean, i.e., northwestern Atlantic, Rocky Mt., Appalachian Mt. and Greenland. Note that some GWs also appear over European regions, e.g., Scandinavia and Scotland, which is too close to the model lateral boundary and thus will not be considered in this study. The GWs over those regions with high terrains are distributed more densely and have higher intensity, which is due to their locked phases from generation to propagation (Fritts and Nastrom 1992). On the contrary, without significant direct topographic impacts, GWs usually occur along the left flank of the upper-level jet in that quasi-stationary trough all through the month, also referring the Atlantic storm-track regions. And the intensity is stronger at the exit-region

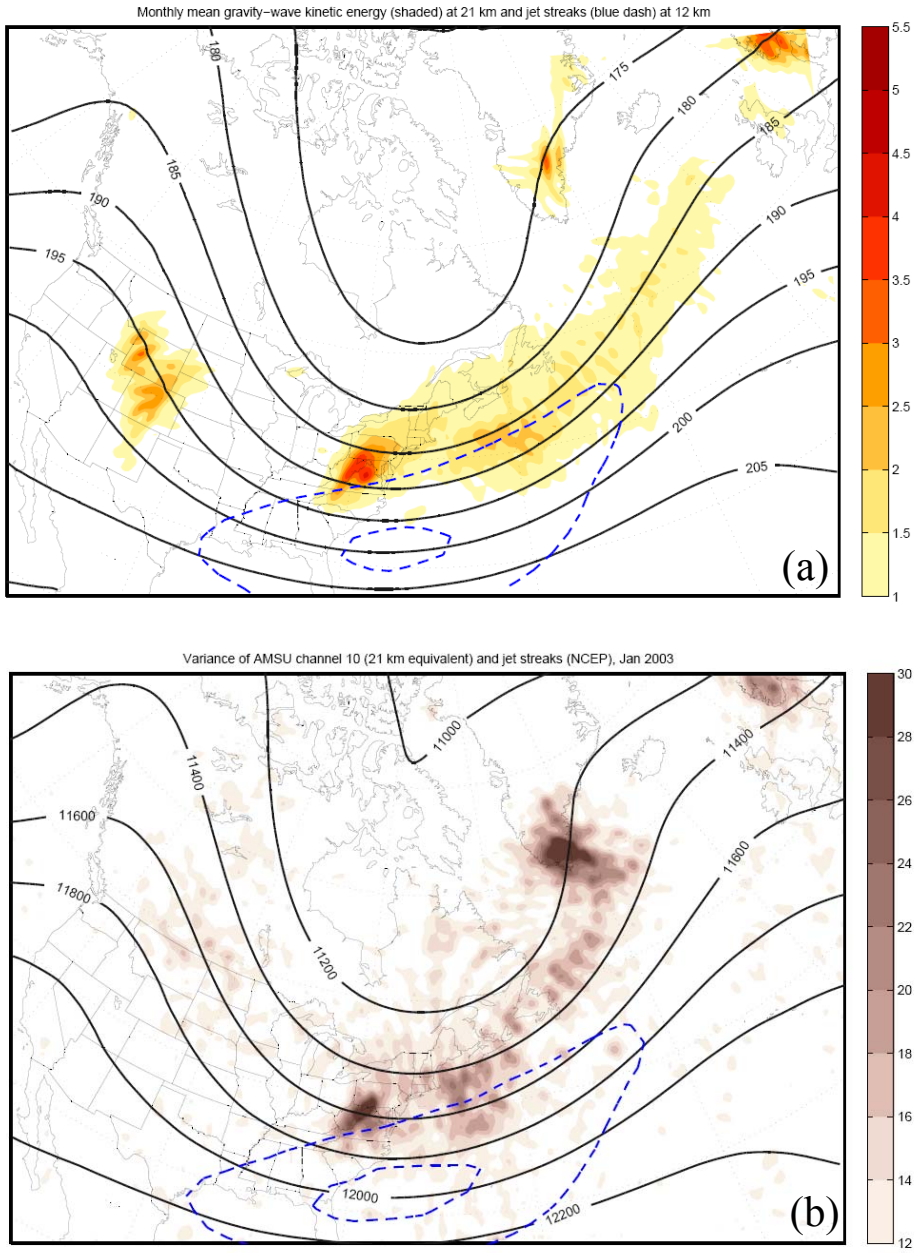

Fig. 1 Monthly mean perturbation kinetic energy (a) at 21 km, in unit of $m^2 s^{-2}$, with jet stream (dashed line) and pressure (solid line) at 12 km; and monthly AMSU-A radiance variance (b) at channel 10, in unit of K^2, with mean background flows at 300 mb. The contours of jet are at 45, 55, 65 m/s.

of the jet, so that it is considered as the source area of such type of GWs, and become weaker at downstream during their propagations.

To verify the model-derived GW climatology results, monthly variance map of AMSU-A radiance is shown on channel 10 (Fig.1b, 21-km height equivalent). According to one-month comparison, we find significant agreements between AMSU-observed GW activities and model-derived results, as the same as the main background flows that derived from daily NCEP FNL analyses. The major observed GW favorite regions mostly have the same patterns and intensity variations as those raised in model results, only except Rocky Mt. areas, where only very weak GW signals appear on AMSU-A map. However, in previous observational works, GWs over the Rockies are significantly obtained by other measurements, i.e., aircraft data (Fritts and Nastrom 1992), high-resolution radiosonde (Wang and Geller 2003) and GPS occultation sounding (Tsuda et al. 2000). And for the other regions, corresponding evidences could also be found in literature (refer to Alexander 1998, Plougonven and Zeitlin 2003 etc.).

The lack captures of AMSU data on GWs over Rockies is partially because of the mismatch between AMSU horizontal resolution and GW wavelength. Based on the analysis of GW characteristics, relatively small wavelength (below 200 km) is found for the GWs over Rocky Mt. areas, while they are usually about 300 km or more for northwestern Atlantic, Appalachians and Greenland (not shown). However, NOAA AMSU-A's scan swath is about 2300 km for each cross-track, whose footprint size varies from 50 km at nadir to 110 km at outmost range (Wu and Zhang 2004, Eckermann and Wu 2006). And the Rocky Mt. areas are not well covered by AMSU-A cross tracks, where such GW active region usually located at coarse resolution ranges or intervals

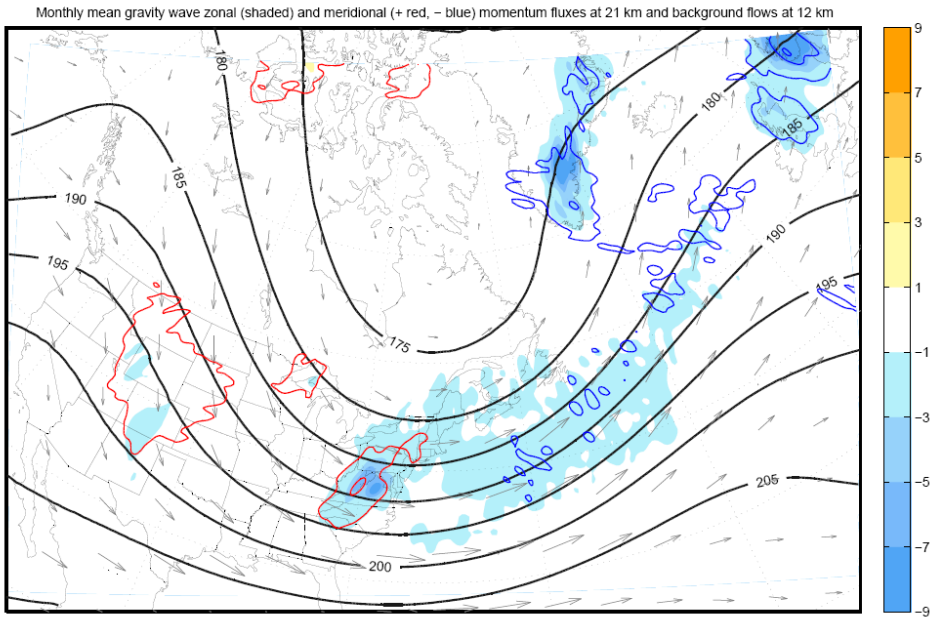

Fig.2 Monthly mean zonal (shaded) and meridinol (contour, positive in red and negative in blue, with interval of 4) momentum fluxes at 21 km, in unit of $x10^{-2}$ m^2 s^{-2}.

between those scan tracks. Hence those GW is hardly to be captured by AMSU observations, considering whose average resolution (footprint size) is about 100 km, which is also confirmed in historical analyses of AMSU data extended to 10 years (Jiang et al. 2003). But situation for the other GW regions is much better in this case.

One of the most important impacts of GW is its eddy transport effects on momentum, heat and chemical species: GWs are usually generated by lower atmospheric sources and propagate vertically, finally break up or dissipate at upper levels (stratosphere, mesosphere and lower thermosphere), thereby they could couple the lower and upper atmosphere together and then affect the global distributions of main circulations, temperature and other atmospheric species (Fritts and Alexander 2003). For instance, without small-scale wave forcing, the stratospheric polar vortices would be much stronger and the temperature in the polar upper stratosphere would be much colder (Hamilton et al. 1994). Considering the validity of our simulations against AMSU measurements, we can use those fully resolved three-dimensional grid data to investigate the GW contributions on main flows, and the higher resolution (30km in horizontal and 0.25km in vertical) could provide us further benefits comparing to conventional observations and global models.

Fig.2 demonstrates the zonal and meridional momentum fluxes at 21-km height, where positive (negative) zonal component ($\overline{u'w'}$) means eastward (westward) GW propagation against background flows, and positive (negative) meridional component ($\overline{v'w'}$) means northward (southward) GW propagation. For zonal flux (shaded), strong westward momentum transports arise over those specific regions that consistent with GW energy map (Fig. 1a), their direction is opposite to the eastward background flows (Fig.

1); for meridional flux (contour), northward momentum flux lies over the left branch southward jet streak, and contrarily southward momentum fluxes propagate against the right branch northward jet streak. It is said that, the westward GW drags are significant during mid-latitude winters, especially over the northwestern Atlantic regions, such conclusion is unanimous with the previous studies by Kim et al. (2003).

In fact, such mesoscale processes could not be resolved explicitly in most global models, where GW drag parameterization is often required in practice. Because of the fixed topographic features, the stationary mountain waves forces onto background wind variances are well understood and easier to estimate, which is associated to terrain roughness and horizontal wind speed (Fritts and Nastrom 1992a, Kim et al. 2003). But the situation is more complicated for non-stationary jet-front GWs, as they are indeed dependent on synoptic backgrounds and their source spectrum is not available from current research. Charron and Manzini (2003) propose a simple method on jet-front GW parameterization by using Miller frontogenesis function as a precursor of GW generation, and then estimate its propagation direction and momentum contribution through empirical evidences. However, such method is still far more than sophisticate, where the specifications on generation mechanism, launching level and radiation direction are still under developments.

The above contents demonstrate the favorite GW regions of North America and North Atlantic Ocean and their potential impacts on large-scale circulations. However, the generation mechanisms of those GWs could be quite different. Fig. 3 roughly represents the possible sources of those relevant areas. There are mainly two types of GWs are captured during our studies, topographic GW (Rockies, Appalachians and

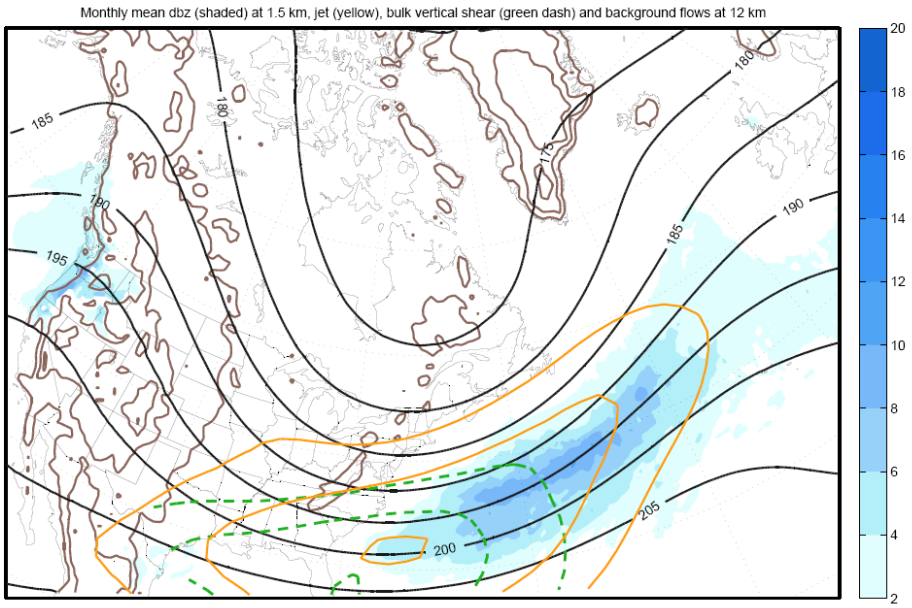

Fig. 3 Monthly mean background flows, including: pressure (black thick) and jet (orange solid, at 35, 45, 55 m/s) at 12 km, bulk vertical shear (dashed green line, at 3.5, 4.0, 4.5 m s^{-1} km^{-1}) between 2 and 12 km and reflectivity (shaded, in unit of dbz) at 1.5 km.

Greenland) and jet-front related GW (northwestern Atlantic). For the first part, we notice that their distribution is obviously terrain dependent, where the terrain roughness (defined as local cell terrain variance, refer to Fritts and Nastrom 1992a) along the wind direction is considerably larger than other places, so that the generation scheme could be evidently addressed as terrain forcing (topographic GWs), though the impacts from the interaction of topography with jet/fronts is very significant. For the second part, which is the key focus of this study, the GWs are excited from non-orography regions, coinciding with strong jet stream, vertical shear and low-level convections. It is said that the jet-front system over Atlantic could be their origin, however, the exact generation mechanism is still unclear since other factors can also play important roles on the GW generation (Fritts and Alexander 2003). Even though the convections have better a pattern that similar to the GWs, nevertheless, the intensive GW energy sourcing region is more likely correlated with the jet streak and vertical shear, where imbalance flows are continuously produced by synoptic-scale waves and subsequently radiate GWs through spontaneous geostrophic/balance adjustment (Uccellini and Koch 1987, Zhang 2004). Further investigations on such topic will be post in the next section on a particular GW event through sensitivity experiments.

4. SENSITIVITY STUDY ON A STRONG JET-FRONT GRAVITY WAVE EVENT

Based on the AMSU-A observations during a month-long period, significant radiance perturbations over northwestern Atlantic are found between 19~21 January 2003, which are induced by large-amplitude GW activities along with strong jet streaks. In this section, a control experiment is performed to reproduce the GW generation and propagation features at their incipient and mature stages from 00Z 19 to 00Z 20 January, and then a set of sensitivity tests with various model settings are conducted to investigate the source mechanisms of these enhanced GWs during this period.

4.1 Control simulation of jet-front gravity wave generation

The control experiment (hereafter CNTL) is initialized at 00Z Jan 18 with the standard model setting (see Section 2.1), where a one-day spin-up time ahead the GW occurrence is placed to allow the baroclinic jet-front system getting developed. The evolution of GWs and their synoptic background is shown in Figs. 4 and 5, including model-derived results and AMSU-A observations at the referenced time. In general, the 30-km MM5 simulations successfully captured the whole process of GW generations over the northwestern Atlantic and Appalachian Mt. regions. At 06Z January 19 (Fig. 4a), a strong jet streak located at the right branch of the major upper-level trough along the east coast, the jet strength is more than 80 m s^{-1} at its core level (i.e., 12 km). Sparse GW activities are represented at both the jet and topographic areas, however, the AMSU-A measurement (Fig. 5a) are not sensitive to those signals due to their relatively short

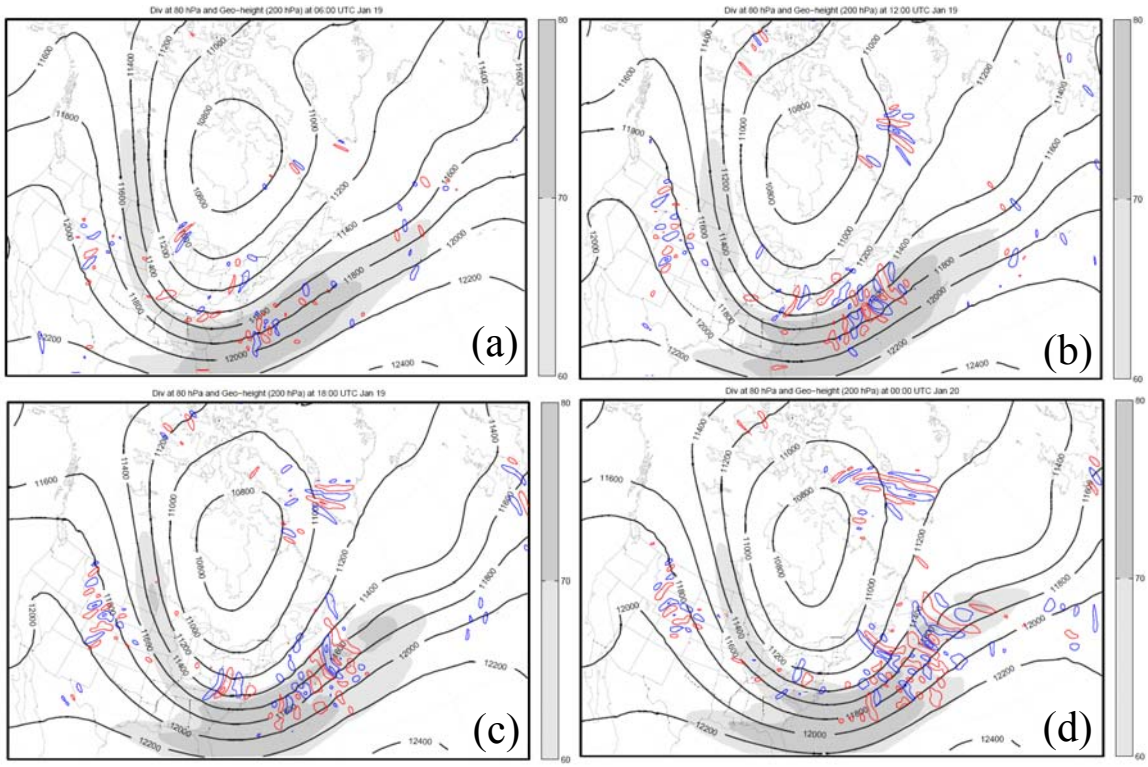

Fig.4 Gravity waves derived from CNTL at (a) 06Z (b) 12Z (c) 18Z (d) 00Z 19~20 January 2003, including 18-km horizontal divergence (negative in red; positive in blue) at 18 km, with intervals of $\pm 5 \pm 15 \pm 25 \times 10^{-5}$ s^{-1}, 12-km pressure (solid line, unit in mb) and jet stream (shaded, unit in m s^{-1}) shown at 12 km.

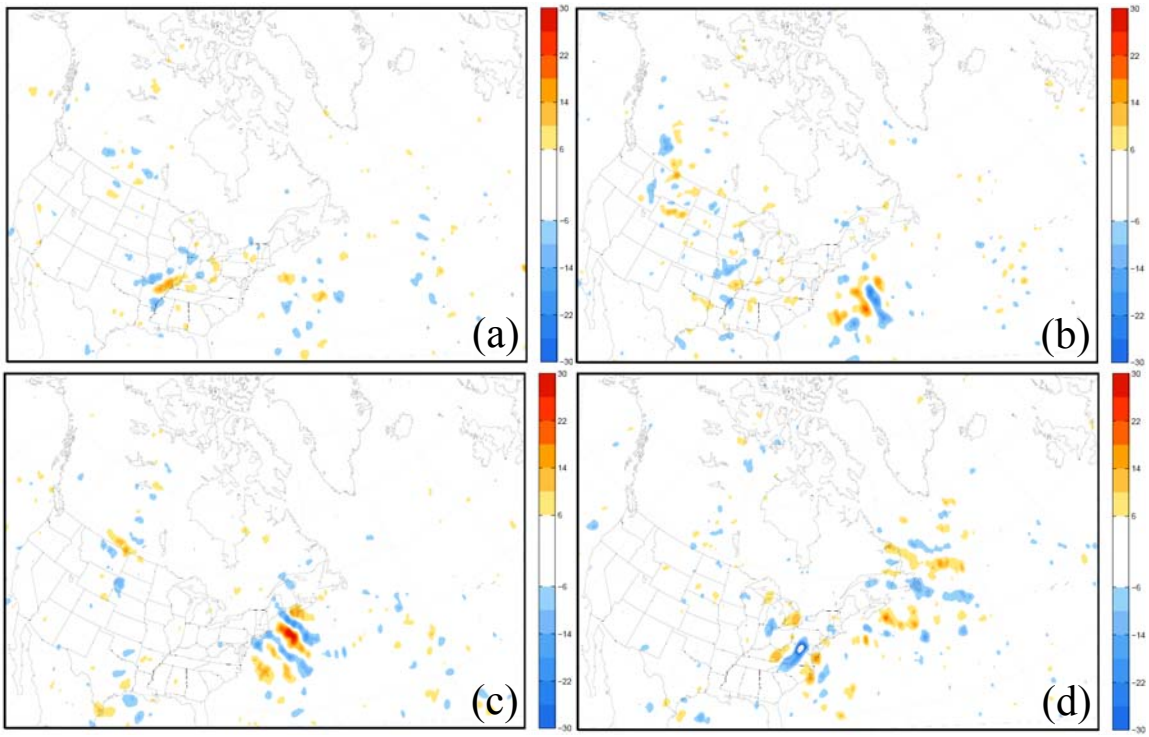

Fig.5 Channel 9 (18-km equivalent) AMSU-A radiance perturbation (shaded, unit in K) shown at (a) 06Z (b) 12Z (c) 18Z (d) 00Z 19~20 January 2003.

wavelength and weak amplitude during the initial stage. After 36-h integration valid at 12Z, significant GWs are excited over the jet streak at West Atlantic, and the AMSU-A data provide a strong agreement on those GW-produced disturbances, both on the location and wave structures (compare Fig. 4b and Fig. 5b). Such jet-related GWs are radiated continuously in the following hours and propagate downstream with the phase track along the jet and energy spreading in perpendicular (Fig. 4c), which subsequently result in the larger AMSU-A radiance perturbations at 18Z (Fig. 5c). At the same time, the major trough moved eastward and let the horizontal wind blew toward the Appalachians and Rockies, meanwhile the topographic GWs were produced instantaneously (Fig. 4c and d). It is also confirmed by AMSU-A maps, even though the peak time is slightly different (Fig.5 d). At 00Z, the GWs over jet streaks reached the North Atlantic region with reduced amplitude, because of the energy dissipation during their propagation, and those weakened signals also reflected by AMSU-A measurements correspondingly (Fig. 5d).

The whole comparisons between the simulations and satellite observations provide us a reasonable confidence that the model successfully reproduced this large-amplitude GW event and its synoptic environment, it also suggest the potential uses of those model products for further investigations, e.g., structuring the generation mechanisms. Note that most GWs are generated from jet-core region and propagate out of the jet exit, which consistently matched with the conceptual model of jet-front GW generation in Uccellini and Koch (1987), accordingly we can believe that such strong GW event could be highly related to its jet-front background and provide us a good opportunity to investigate the specific generation/propagation characteristics of such jet-

front GWs with comprehensive model supports, which is also the major concern of this study.

Figs. 6 and 7 focus on the northwestern Atlantic regions and describe the incipient and mature stages of this jet-front GW case, and unveil both of their horizontal and vertical structures with several source-related variables, such as ΔNBE and reflectivity. As mentioned in Zhang et al. (2001), the residual of NBE (ΔNBE, refer to Section 2.3) is a useful variable that measures the degree of flow deviation from the balanced state, which is also a first order approximation to the tendency of horizontal divergence. The nonlinear balance is used here as it is more appropriate to mesoscale systems (Davis and Emanuel 1992). And such imbalance flows are responsible for generating GWs within jet-front system via spontaneous-emission process (refer to imbalance adjustment, Zhang 2004). However, the GW itself also contributes imbalance signals, so that a low-pass filter with cut-off wavelength of 900 km is applied on ΔNBE for only retaining their synoptic-scale features. On the other hand, convection is known as another source of GW generation, whose scale is much smaller and location could be represented by localized vertical velocity and reflectivity. Fig. 6, 7 could provide us some direct images for those GWs within jet-front system from various sources. By tacking their origins and phase tracks, we can partially distinguish the jet-front GWs from the other surface sources.

At the beginning, the major jet-front system did not move into the concerned region, and only weak imbalance signals are found at upper levels (around 12 km) , which is associated to jet streak and tropopause folding, while isolated convection-induced GWs appeared at 500 km position with smaller wavelength less than 200 km (Fig. 6b). At 06Z, increasing imbalance occurred at middle levels (around 6 km) due to

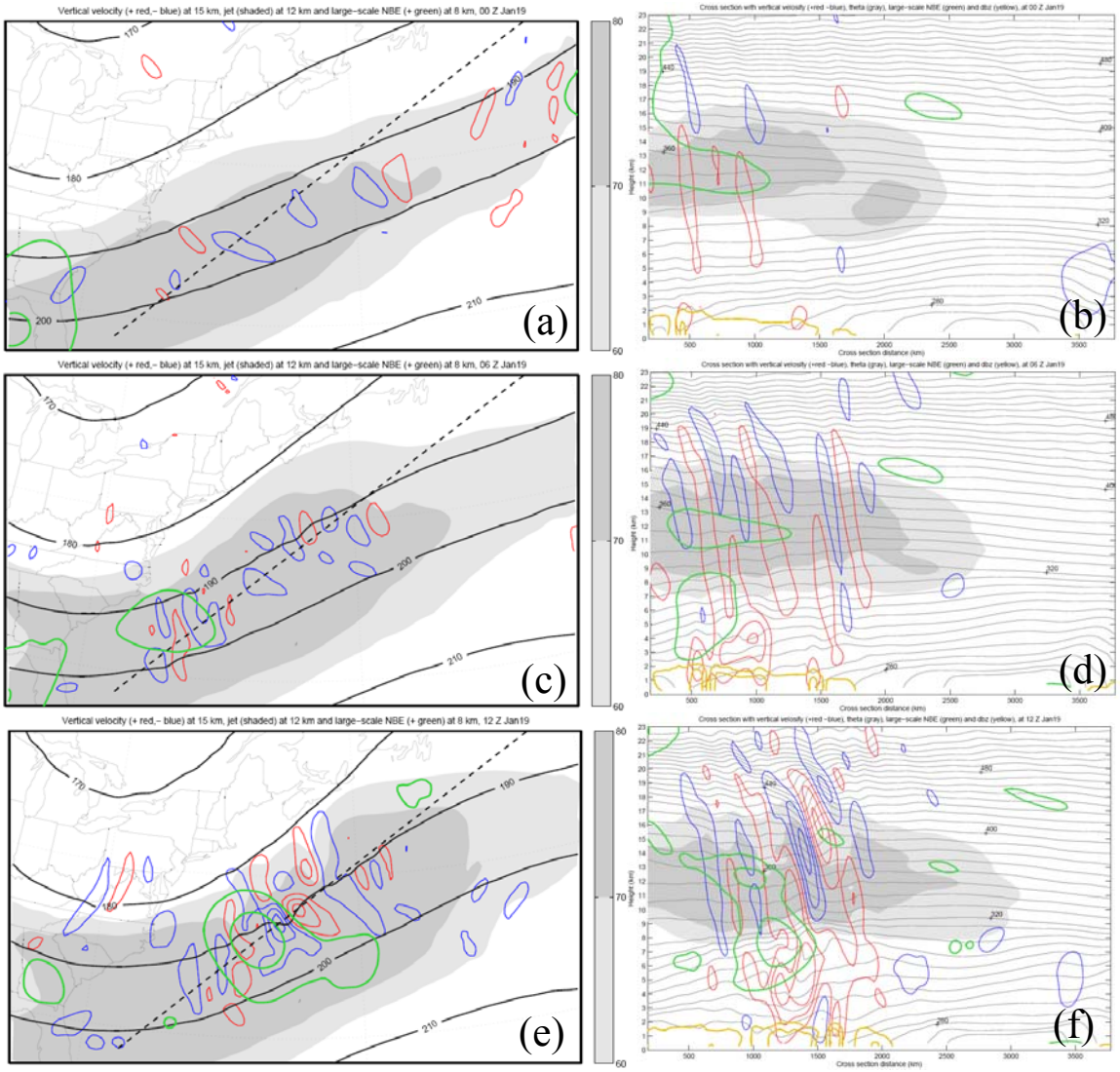

Fig.6 CNTL horizontal (left column, at 15 km) and vertical (right column) structures of incipient jet-front gravity waves, (a) (b) for 00Z, (c) (d) for 06Z and (e) (f) for 12Z, 19 January 2003: including vertical velocity (positive in red, negative in blue) shown at ± 0.05 ± 0.15 ± 0.25 m s^{-1}, 12-km jet stream (shaded, unit in m s^{-1}) and pressure (solid black, unit in mb), reflectivity (yellow) with 20 dBZ interval, large-scale NBE residual (thick green) with 2 x 10^{-9} s^{-2} interval and potential temperature (gray line) with 10 K interval upper 320 K and 4 K interval below. The position of cross section is marked as dashed line.

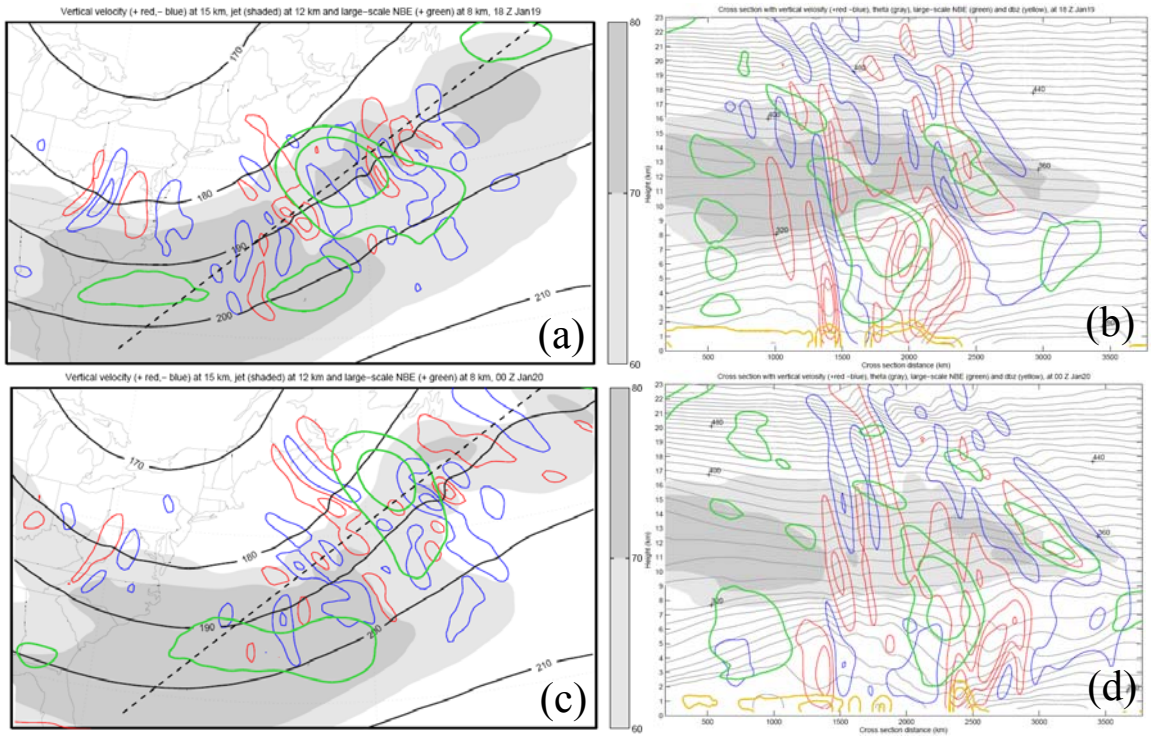

Fig.7 Same as Fig. 6, but for mature stage: (a) (b) for 18Z 19 January 2003, (c) (d) for 00Z 20 January 2003.

the strengthening baroclinicity and frontogenesis at lower-levels, where large-scale updraft, horizontal temperature gradient and moisture convergence are identified (Fig. 6d). At the meantime, some GWs started to be radiated from the imbalance source with the wavelength of 400 km, however, convection-GW could be also involved at this time. In the next 6 hours, larger ΔNBE and GW amplitude are shown both on horizontal and vertical plots (Fig. 6e and f), it implies that the continuous imbalance increasing could sustain the jet-front GW generation and amplify their intensity. And the imbalance flow is determined by baroclinic instability during the development of synoptic jet-front system. We notice that the jet-front GW actually propagated downstream and vertically (combined with basic flows) just from its origin that labeled at maximum ΔNBE areas around 8-km, rather than any other surface sources, which addressed the same pattern as those idealized results in Zhang (2004). However, the surface frontogenesis could not be excluded after all, because its close associations with baroclinic development and imbalance production are crucial for the GW generations, and it also could be linked to the maintenance and enhancement on those jet-front GWs (refer to Section 4.2).

In the last 12 hours (Fig. 7), the jet-front system moved northeastward and produced large-scale imbalance persistently, while jet-front GWs turned to be dissipated with extended phased rests and enlarged wavelength (about 600 km), and propagate more likely toward horizontal direction (Fig. 7b, d). It indicated that the propagation of jet-front GW would meet the critical level at 15~16 km and then have their wave properties changed. The critical level is defined as the level at which the vertically sheared basic flow is equal to the horizontal phase speed of the wave. The vertical wavelength decreases as the wave packet approaches the critical level, so that the wave energy could

be absorbed quickly by model diffusion and then can not be transported upward after that (refer to Lin 2007, Section 3.8). Therefore, the further consideration of such situation is important for the estimation and/or parameterization of jet-front GW momentum flux that contributes to stratosphere and mesosphere circulations in much higher levels. On the other side, some convection-induced GWs still raised with shorter wavelength (200 km) and apparent low-level sources, e.g., at 1500 km position (Fig. 7b, d). They propagate quickly in vertical, but produce much smaller energy spreading normal to the phase track in horizontal, i.e., their phase rest extension is much smaller than those of jet-front GWs (Fig. 7c).

In summary, jet-front GW radiated from maximum imbalance regions (ΔNBE core) at middle and upper levels are clearly identified in this strong GW event, even though convection-GW is still involved with. The increasing imbalance flow from baroclinc background could maintain such GW generations through the adjustment process (Zhang 2004, Wang and Zhang 2007). And surface frontogenesis could be also counted for imbalance production. The jet-front GWs would be dissipated if critical level occurs after their mature stage, such level is confirmed at 15~16 km and similar with its idealized criteria in Zhang (2004).

4.2 Sensitivity experiments

Four parallel sensitivity experiments are scheduled in this section to test the conclusions that derived from CNTL and also provide additional information to purify generation mechanism of jet-front GW from the other sources. They are: 1) a fake-dry

experiment without latent heat releasing with 30-km grids, named “30DRY”; 2) a higher resolution experiment with 10-km grids, as “10KM”; 3) another fake-dry experiment but with 10-km grids, as “10DRY”; 4) a very coarse resolution experiment with 120-km grids, about 1 x 1 degree, which is comparable to those global models, named “120KM”. The other model conditions are exactly the same as those in CNTL.

In 30DRY experiment, the latent heating associated with the phase change process of water substances is disallowed, which could largely depress those localized convective activities and therefore remove the convection-induced GWs. Accordingly, we note that those short-wavelength GWs did not appear at the beginning time (compare Fig. 8a, b and Fig. 6a, b). Moreover, the large-scale updraft was also reduced in 30DRY (Fig. 8d), so as the horizontal temperature gradient at middle and lower levels, such reduction of baroclinicity could finally result in the slower development of jet-front system and also the weaker imbalance flows (reduced by 1~2 x 10^{-9} s^{-2} in 30DRY, about 50%), even thought the jet streak is still as strong as CNTL. Therefore, the jet-front GW generations were delayed by 12 hours, but those GWs still could be excited with preserved properties after the slow development of baroclinic system. As in Fig. 8e and f, strong jet-front GWs are directly emitted from the upper-level imbalance maximum, with 400 km wavelength and propagating downstream and vertically. Because of the changed large-scale environment in 30DRY, the critical level did not appear for that time. Consequently, this experiment proves the existence of jet-front GW generation via imbalance adjustment, and also indicates that convection is not the factor for such type of GW generation.

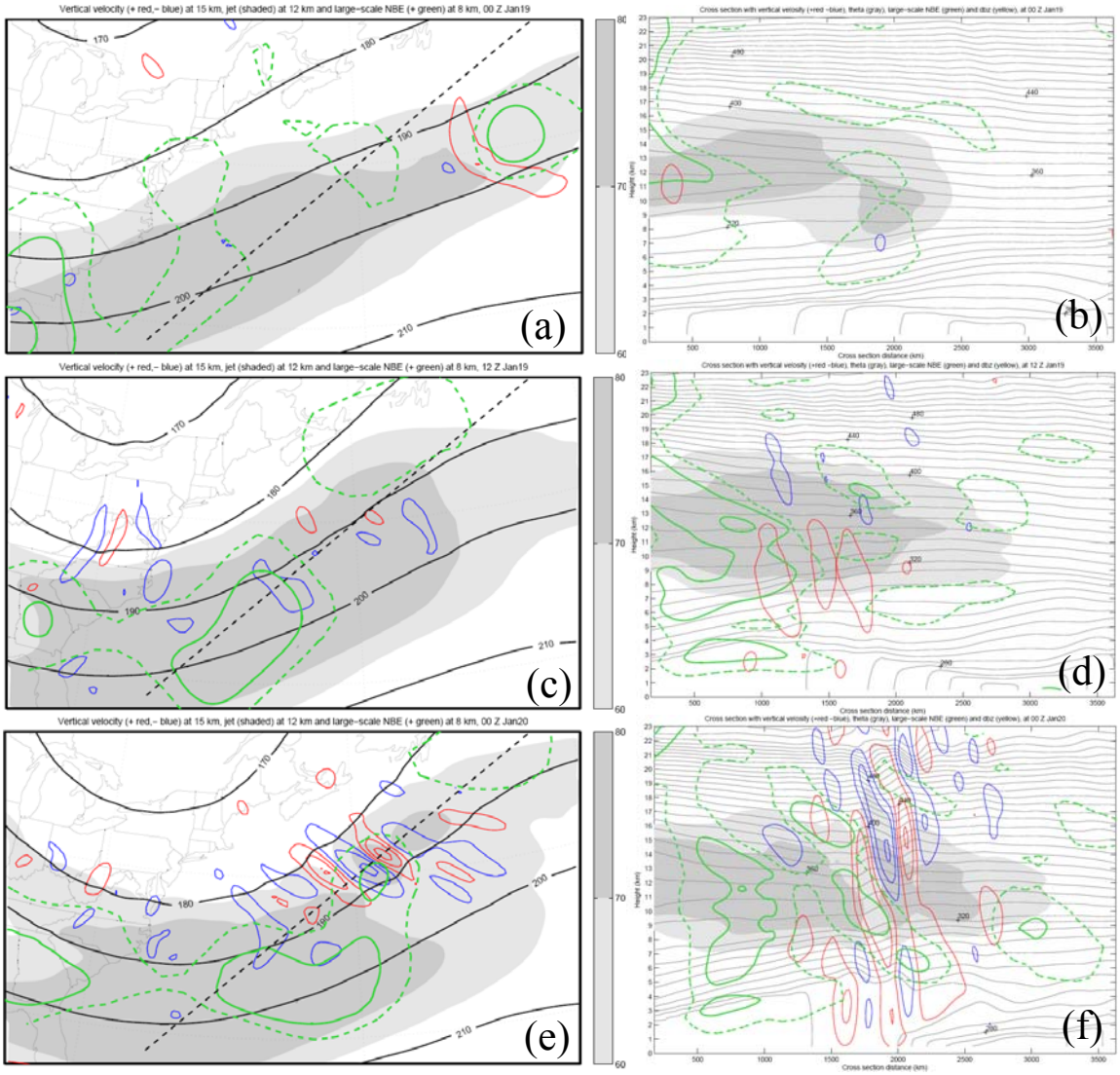

Fig.8 30DRY experiment at 00Z (a) (b), 12Z (c) (d) 19 January and 00Z (e) (f) 20 January 2003: the legends are the same as Fig. 6. Additional line of NBE residual added at 1 x 10^{-9} s^{-2} (dashed green line).

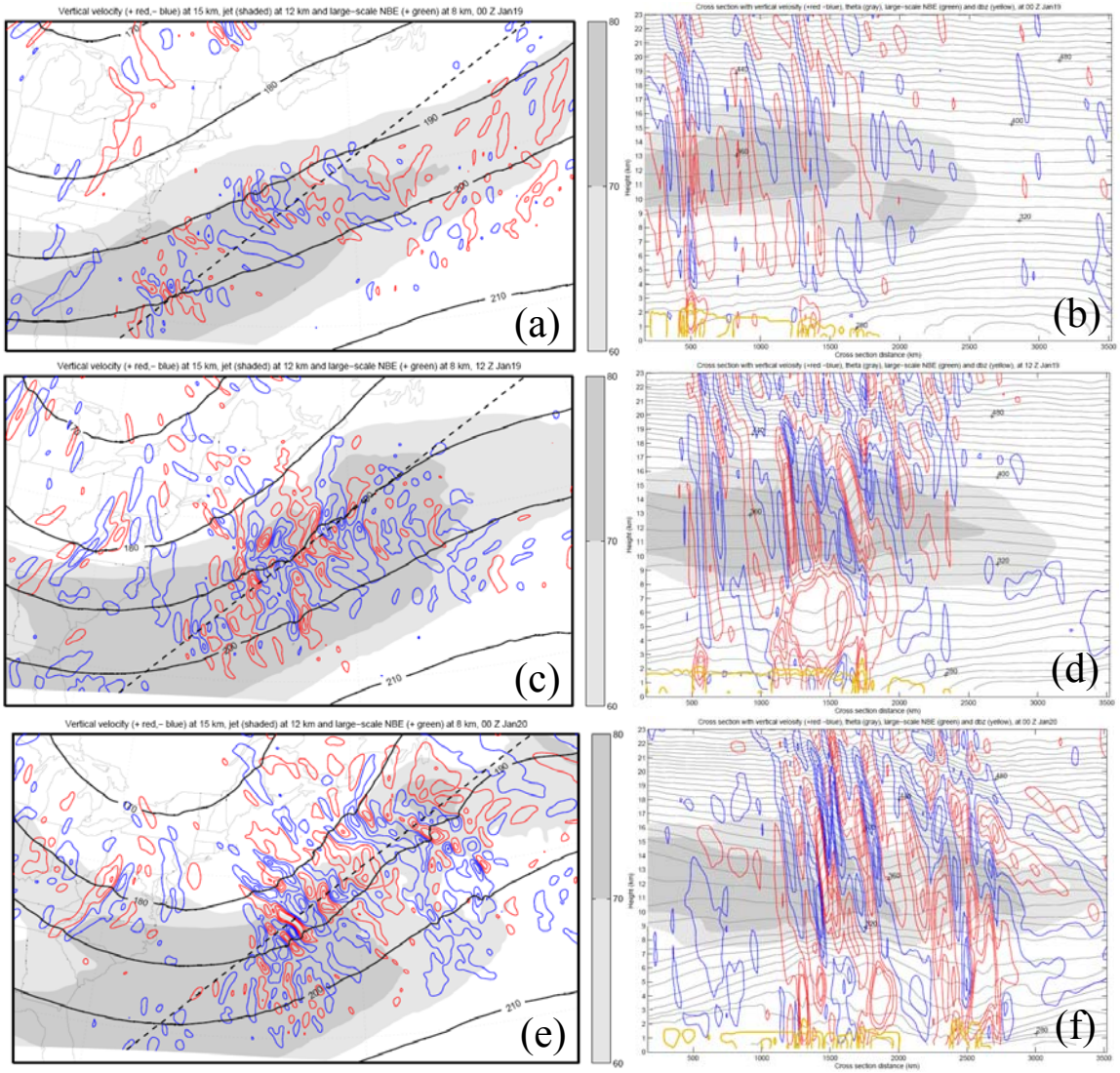

Fig.9 Same as in Fig. 8 but for *10KM* experiment and without large-scale NBE residual.

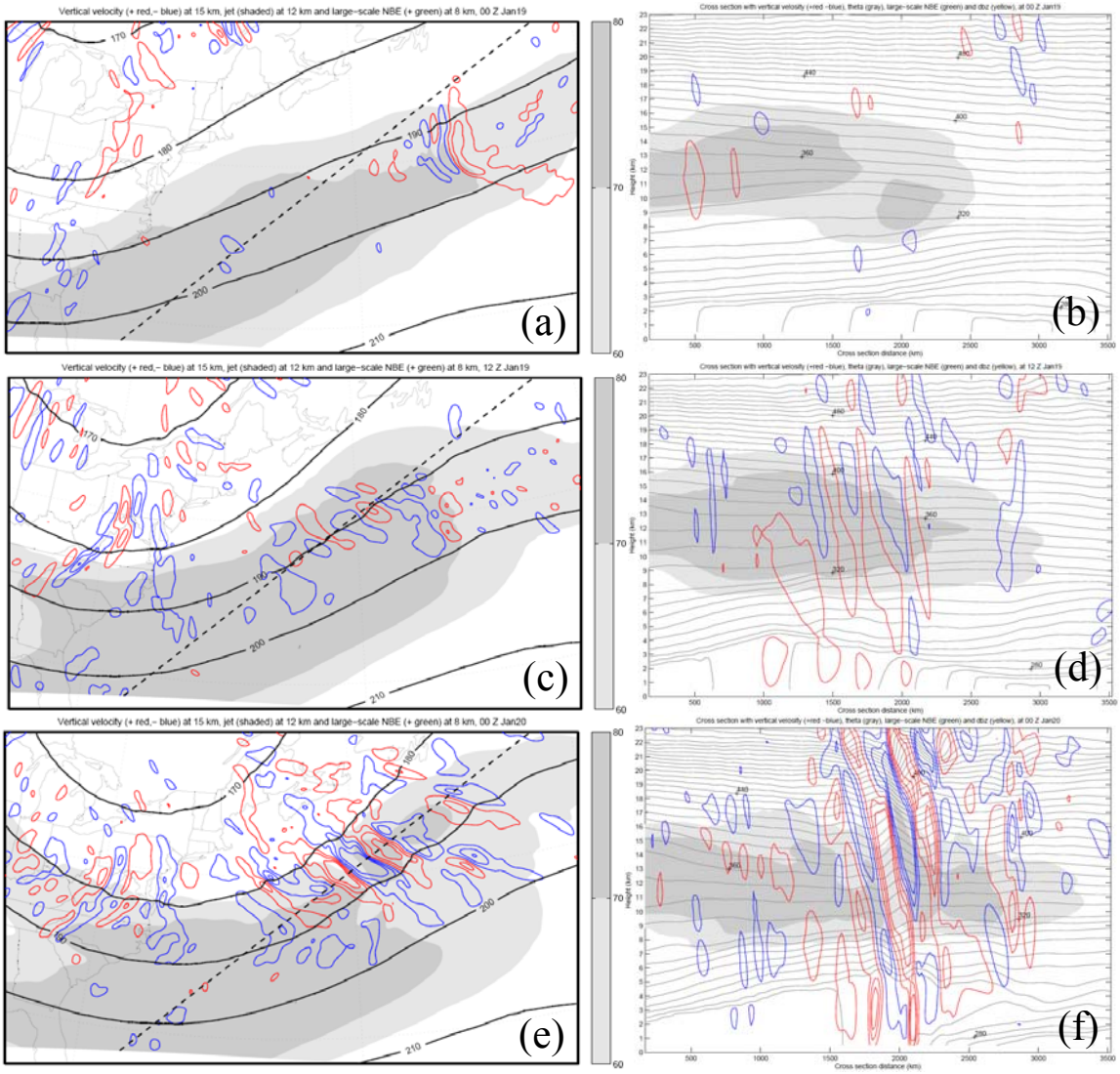

Fig.10 Same as in Fig. 8 but for *10DRY* experiment and without large-scale NBE residual.

On the contrary, 10KM experiment is set to enhance the convections through the finer resolution, where more convective motions could be represented explicitly in that. The same horizontal and vertical plots are provided in Fig. 9, we can find that convection-induced GWs were generated quickly in 10KM, even at its beginning time (Fig. 9a). And those convection-GWs are strongly scale dependent, because smaller wavelength, about 100~200 km, is identified comparing those with 200 km scale in CNTL, considering 100-km waves are hardly captured by CNTL. Actually, the jet-front GWs still could be distinguished with the same wave characteristics and origins as in CNTL, even though they are highly combined and disturbed by convection-GWs (Fig. 9d, f). In order to make it more clearly, 10DRY is performed to remove those convection-GWs and then seperate the jet-front ones. As in 30DRY, under the same baroclinic background, those convection-related small-scale perturbations are eliminated both in incipient and mature stages of such jet-front system, however, the most important feature of 10DRY is that the same characteristics of jet-front GWs are consistently generated as those coarse-resolution products (Fig. 10e, f), hence it is reasonable to conclude that the jet-front GW generation is an inherent dynamical mechanism only related to the upper-level imbalance that derived from baroclinic environment, rather than an offspring of particular model resolution or convective perturbations. Another, the amplitude of jet-front GW is much larger in 10DRY, comparing to the 30-km results (refer to Fig. 6f, Fig. 8f and Fig. 9f), but as the same as 10KM, so that the intensity of jet-front GWs could be model-scale related, which also determine the total amount of the momentum flux from jet-front GW transports.

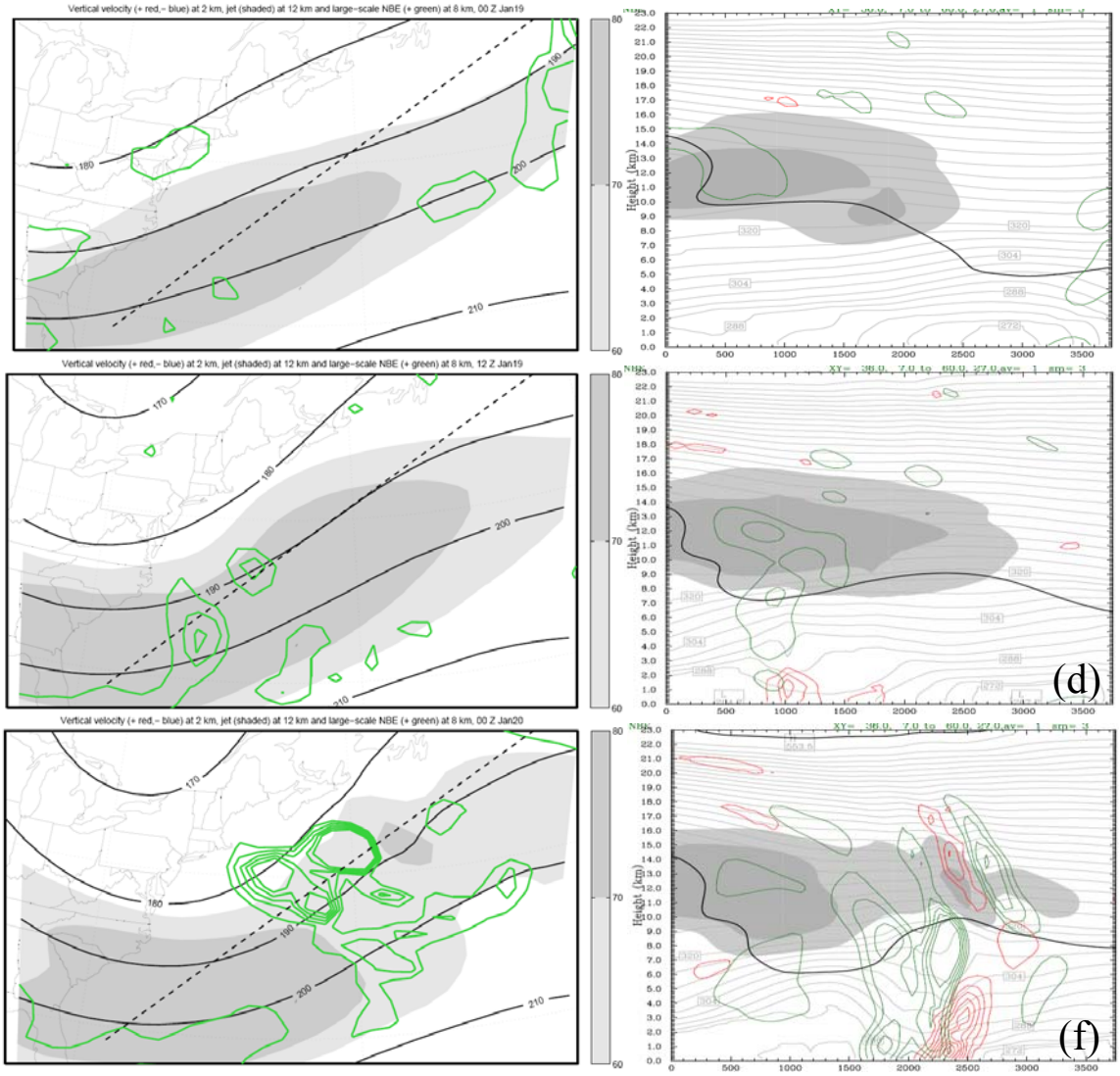

Fig.11 The *120KM* experiment at 00Z (a) (b), 12Z (c) (d) 19 January and 00Z (e) (f) 20 January 2003: horizontal (left column, 8 km) and vertical (right column) NBE residual (green line) with 2 x 10^{-9} s^{-2} interval, Miller frontogenesis function (red line) shown in vertical with 0.2 K (100 km h)$^{-1}$ interval, and dynamical tropopause (thick black) labeled at 1.5 PVU. 8-km jet stream (shaded) and potential temperature are labeled as same in Fig. 6.

At last, a much lower resolution experiment, 120KM, is conducted to demonstrate the evolution of the pure large-scale background during this case, where the 120-km grids are not sufficient to resolve mesoscale GWs or other small-scale perturbations explicitly. In Fig. 11, the gridded ΔNBE structures are mostly the same as those filtered results in CNTL. And as no filter is applied in 120KM, its peak values of ΔNBE core are larger than CNTL. Moreover, the frontogenesis function (Miller 1948; Hoskins 1982) and dynamical tropopause are also shown in Fig. 11. Based on the different ΔNBE cores appeared at various positions, it is demonstrated that the production of imbalance flow is associated with both the surface front and tropopause folding. But they usually contribute together for the total imbalance and subsequently responsible for the continuous jet-front GW generations (Fig. 11f). On the other hand, Charron and Manzini (2003) tried to use low-level frontogenesis function as a predictor for jet-front GWs, and then parameterized their wind variance contributions in global model. However, in our study, large-scale Δ NBE could be a better indicator for the potential uses on jet-front GW parameterization, because that: 1) the ΔNBE maximum is more near to the origin of those waves, and could point out their propagation direction; 2) the ΔNBE is a more direct dynamical variable that related their generation mechanism, i.e., imbalance adjustment; 3) ΔNBE forced GWs could be resolved quantitatively through adding a wave equation and scaling method onto governing equations (Plougonven and Zhang 2007), which provides a more reasonable way for GW parameterization than those empirical methods.

Before the future application of jet-front GW parameterization in large-scale models, we could firstly measure the amounts of momentum fluxes from both jet-front GWs and convection-GWs in CNTL. Based on the wave characteristics that generalized

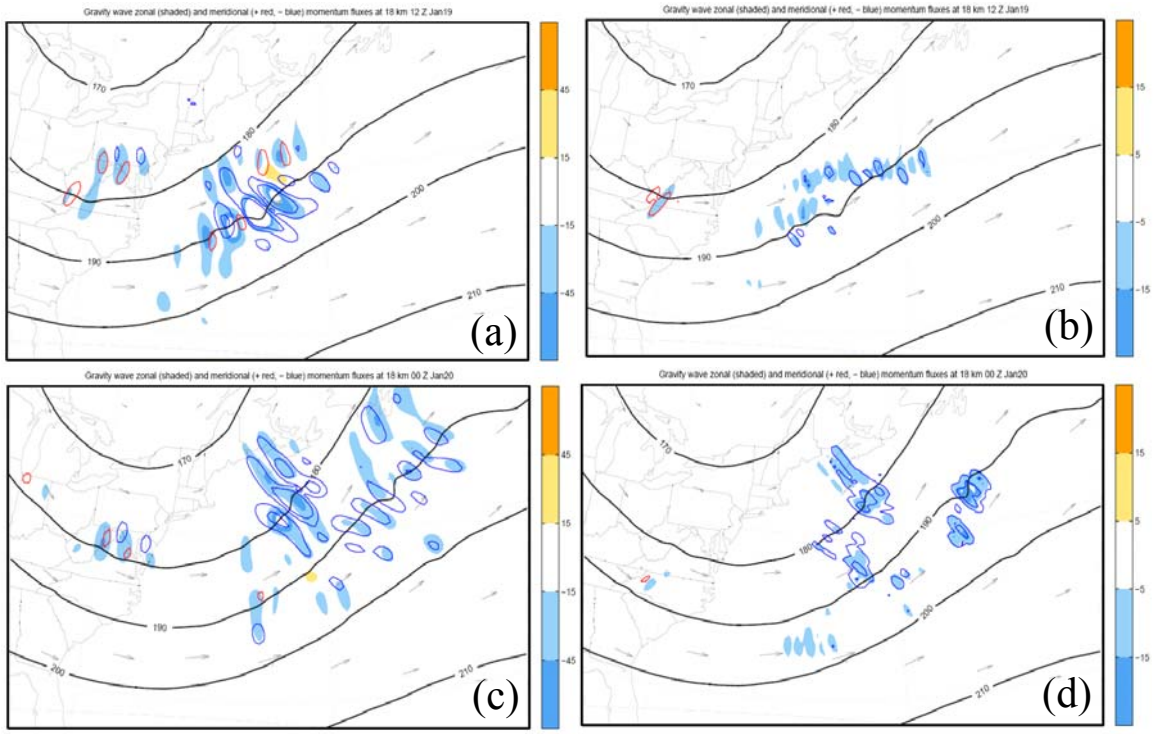

Fig.12 18-km zonal (shaded) and meridional (positive in red, negative in blue) momentum flux of jet-front GW (left column) and convection-GW (right column) in CNTL, shown at (a) (b) 12Z January 19 and (c) (d) 00Z January 20 2003. The intervals are 30 m^2 s^{-2} for left column, and 10 m^2 s^{-2} for right column.

from section 4.1, we use a band-pass filter to extract the perturbations that associated with these two types of GWs, as 200/600 km and 100/200 km cut-off wavelength, respectively. The zonal and meridional quantities are shown in Fig. 12. Notice that the main southwestward momentum fluxes are demonstrated for both of them, which prorogate against the basic jet stream. And the total amount of jet-front GWs is much more significant than convection-GWs in this case, considering their higher values and larger impact areas (Fig. 12). Therefore, it is more important to involve the jet-front GWs into the global models, otherwise underestimation of the forces on stratospheric and mesospheric circulations would be resulted from the absence of jet-front GW consideration. Moreover, the overall contributions mode GW momentum flux from a month-long statistics has been shown in section 3, where jet-front GWs are the major part for the total contributions (refer to Fig. 2).

5. SUMMARY AND DISCUSSIONS

The jet-front gravity waves are one of the most important mesoscale processes that widely exist in the upper tropospheric jet exit region of midlatitude baroclinic systems. Numerous observational and modeling studies have been conducted to reveal the generation mechanism of such waves. Following the idealized simulations of Zhang (2004) and a case study using remote sensing technique of AMSU-A measurement in Wu and Zhang (2004), a month-long real-data simulation is performed through a mesoscale model MM5 with 30-km grid resolution. A typical winter month of January 2003 with strong gravity wave activities is examined, when the jet streams are strongest of the year.

Based on statistical analyses of the monthly total of the model-derived GW kinetic energy and AMSU-A observed radiance variance, both of which represent the disturbance intensity of gravity waves, four regions over North America and North Atlantic Ocean are confirm as favorite places of strong gravity wave activities, i.e., northwestern Atlantic, Rocky Mountains, Appalachian Mountains and Greenland. The first one is related to midlatitude baroclinic jet-front system, and the others are collocated to those great terrains. One of the most important impacts of gravity wave is its transport of momentum, heat and chemical species. We first calculated the monthly mean zonal and meridional momentum fluxes from the montly-long MM5 simulation. Significant anti-background momentum contributions are found in the region of strong jet-front gravity waves, exerting a significant drag to the basic flow at the upper troposphere and the lower stratosphere. Such waves could propagate into much higher levels, and then

become the key driven forces for the main circulations in the mesosphere or higher when they break.

Further sensitivity studies focus on a strong jet-front gravity wave event is conducted to investigate the possible source mechanisms of the gravity waves. A control experiment initialized at 00Z 18 January 2003, and four parallel sensitivity experiments with various microphysics and grid resolution settings are performed. Based on the diagnostics of horizontal and vertical structures of vertical velocity and large-scale imbalance, significant mesoscale gravity waves radiated from the maximum Δ NBE regions are clearly identified in all simulations. Increasingly unbalanced flows from the baroclinic jet-front system could maintain such wave generation through balance adjustment process (Zhang 2004). Both the surface frontogenesis and the tropopause folding can lead to imbalance production. The jet-front gravity waves would be dissipated if critical level occurs (at ~15-16 km in this study). All these results from this real-data case study have provided further supports to those conclusions derived from idealized simulations of Zhang (2004).

Additional evidences from sensitivity test are obtained to prove the dynamical nature between jet-front gravity wave generation and the large-scale imbalance at upper tropospheric jet streak regions, by excluding the convection and model resolution impacts. However, the intensity of such mesoscale waves would be dependent on model resolutions, where high-resolution simulations could resolve more proportion of those sub-grid features and then enhance the wave amplitude. The validation of the realistic wave properties should be implemented between intensive observations and simulations in terms of the same quantities.

Another issue is the parameterization of jet-front gravity waves, which is important because of its significant impacts on momentum transport of the general circulation. In this study, the ΔNBE is suggested as a better indicator to predict the timing and location of jet-front gravity wave generation/propagation rather than Miller frontogenesis function (Chraron and Manizi 2003), considering its advantages of dynamical associations with the generation mechanism of such waves. However, there are still several unsolved problems, such as the critical values to trigger the gravity waves, the total amount of momentum fluxes (could be highly resolution dependent), the wave property changing during propagation (e.g., critical level problem) and the strength/weakness between empirical and explicit methods. After all, the first step for this task is use high-resolution mesoscale simulations and also plenty of observations to structure the characteristics of jet-front gravity waves and its generation mechanism, just like the studies in this manuscript.

Moreover, intensive flight in-situ observations on dynamical, chemical and microphysical quantities with very high resolution could be used to observe gravity wave activities over upper troposphere and lower stratosphere regions. Koch et al. (2005) demonstrated a comprehensive application of the flight data from research aircrafts that focus on turbulence and gravity waves over upper-level jet streak regions, where clear-air turbulence and small-scale waves were both detected through spectral, wavelet and structure function analyses. Therefore, the undergoing field experiment of *Stratosphere-Troposphere Analyses of Regional Transport* (START08), which is scheduled from April to June 2008 to study the chemical and transport characteristics of the extratropical upper tropospheric and lower stratospheric (ExUTLS) region using the NSF/NCAR HIAPER

aircraft, provide us a great opportunity to verify and investigate the jet-front GW generation and propagation in realistic scenario. During the field experiment, a real-time forecast system based on Ensemble Kalman Filter (EnKF) data assimilation is implemented to provide specialized ensemble and high-resolution forecasts for the daily flight operations (see to Appendix), e.g., forecasts of tropopause folding, gravity waves etc.

Based on the preliminary results from START08, significant gravity wave activities are captured both by flight-based measurements and numerical simulations, including various generation sources, such as jet streaks of baroclinic jet-front system and Rocky Mountains. The similar diagnostic methods from Koch et al. (2005) could be used for START08 flight data, where one of the research flights is scheduled for a gravity wave event over Central U.S. and Rockies. Fig. 13 demonstrates a snapshot of START08 scenarios of such gravity waves, and more and more in-situ measurements are undergoing along with the program till June 2008. Combining flight observations and model simulations, we expect to get some further evidences for jet-front gravity waves and their specific features and favorite dynamical environments in future studies.

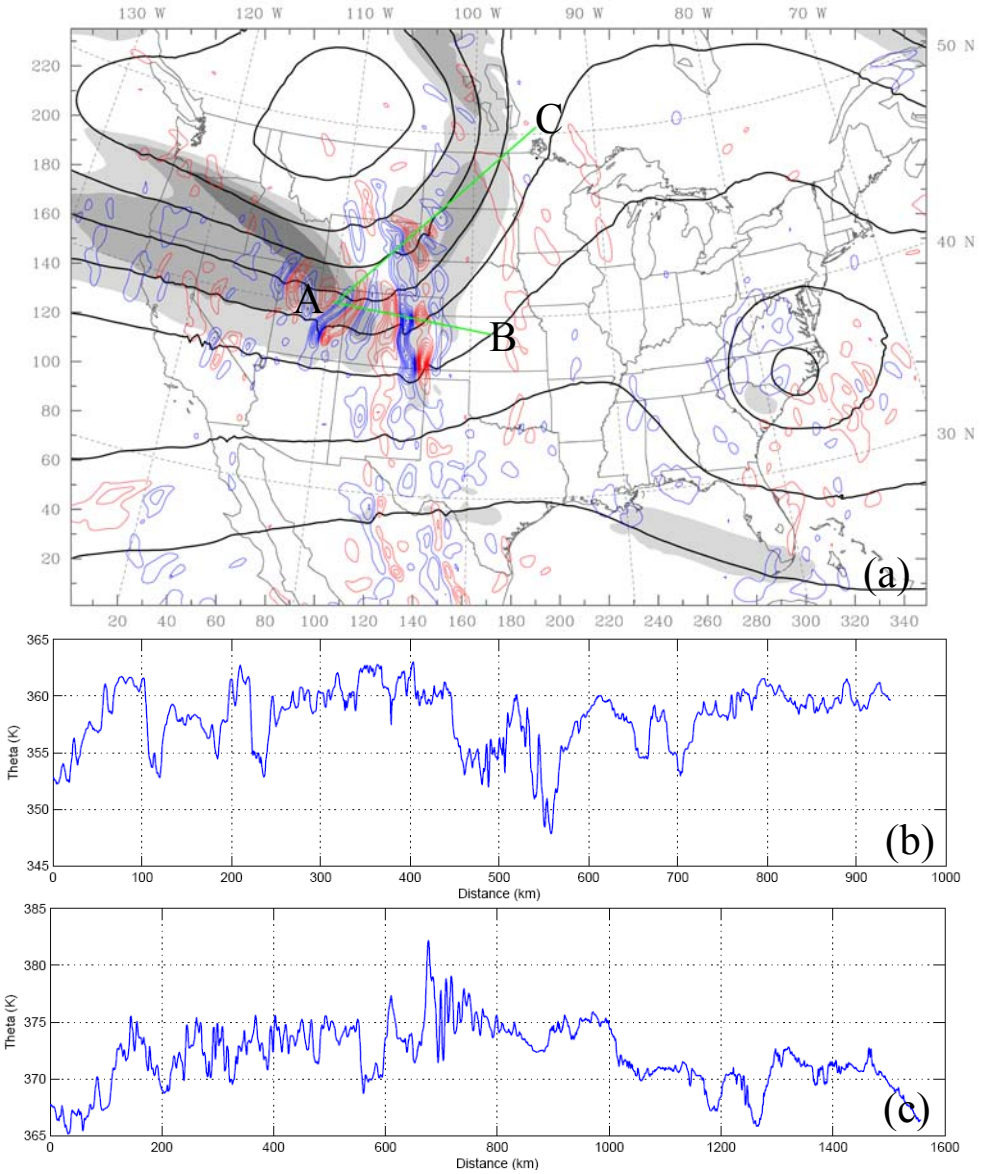

Fig.13 Flight-based measurements and numerical simulations from START08: (a) 15-km forecast valid at 22Z 21 April 2008, for 12-km (around flight height) vertical velocity (positive in red, negative in blue, with 0.03 m s^{-1} interval), 9-km pressure (solid, unit in mb) and jet (shaded, with 10 m s^{-1} interval), flight track marked as AB and AC (thick green line); flight-observed potential temperature (K), for AB (b) and AC (c) during reference time.

REFERENCES

Bosart, L. F., W. E. Bracken, and A. Seimon, 1998: A study of cyclone mesoscale structure with emphasis on a large-amplitude inertia-gravity wave. *Mon. Wea. Rev.*, **126**, 1497-1527.

Charron, M., and E. Manzini, 2002: Gravity waves from fronts: Parameterization and middle atmosphere response in a general circulation model. *J. Atmos. Sci.,* **59,** 923–941.

Davis, C. A., and K. A. Emanuel, 1991: Potential vorticity diagnosis of cyclogenesis. *Mon. Wea. Rev*., **119**, 1929–1952.

Fritts, D. C., and G. D. Nastrom, 1992: Sources of mesoscale variability of gravity waves. Part II: Frontal, convective, and jet stream excitation. *J. Atmos. Sci.,* **49,** 111–127.

Fritts, D. C. and M. J. Alexander, 2003: Gravity wave dynamics and effects in the middle atmosphere. *Reviews of Geophysics*, **41**, 1003-1063.

Gill, A.E, 1982: *Atmosphere-ocean dynamics*, Academic Press, New York, 488 pp.

Griffiths, M., and M. J. Reeder, 1996: Stratospheric inertia-gravity waves generated in a numerical model of frontogenesis. I: Model solutions. *Quart. J. Roy. Meteor.Soc.,* **122,** 1153–1174.

Grell, G. A., 1993: Prognostic evaluation of assumptions used by cumulus parameterizations. *Mon. Wea. Rev*., **121**, 5–31.

Grell, G. A., J. Dudhia, and D. R. Stauffer, 1994: A description of the fifth-generation Penn State/NCAR Mesoscale Model (MM5). Tech. Note TN-3981IA, National Center for Atmospheric Research, Boulder, CO, 125 pp.

Hamilton, K., 1996: Comprehensive meteorological modeling of the middle atmosphere: A tutorial review, *J. Atmos. Terr. Phys*., **58**, 1591– 1627.

Hong, S.-Y. and H.-L. Pan, 1996: Nocturnal boundary layer vertical diffusion in a medium-range forecast model, *Mon. Weather Rev*., **124**, 2322–2339.

Jiang, J. H., S. D. Eckermann, D. L. Wu, and J. Ma (2004), A search for mountain waves in MLS stratospheric limb radiances from the winter Northern Hemisphere: Data analysis and global mountain wave modeling, *J. Geophys. Res.,* **109**, D03107, doi:10.1029/2003JD003974.

Kim, Y.-J., S. D. Eckermann, and H.-Y. Chun (2003), An overview of the past, present and future of gravity-wave drag parameterization for numerical climate and weather prediction models, *Atmos. Ocean*, **41**, 65– 98.

Koch S. E., and P. B. Dorian, 1988: A mesoscale gravity wave event observed during CCOPE. Part III: Wave environment and probable source mechanism. *Mon. Wea. Rev.*, **116**, 2570–2592.

Koch, S. E., and C. O'Handley, 1997: Operational forecasting and detection of mesoscale gravity waves. *Wea. Forecasting*, **12**, 253–281.

Koch S.E., Jamison B.D., Lu C.G., Smith T.L., Tollerud E.I., Girz C., Wang N., Lane T.P., Shapiro M.A., Parrish D.D., Cooper O.R. 2005: Turbulence and gravity waves within an upper-level front, *J. Atmos. Sci.*, **62**, 3885-3908.

Krishnamurti, T. N., 1968: A diagnostic balance model for studies of weather systems of low and high latitudes, Rossby numbers less than one. *Mon. Wea. Rev*., **96**, 518–530.

Lin, Y. and F. Zhang, 2008: Tracing mesoscale gravity waves in baroclinic jet-front

systems. *J. Atmos. Sci.*, In press.

Loughe, A. F., C.-C. Lai, and D. Keyser, 1995: A technique for diagnosing three-dimensional ageostrophic circulations in baroclinic disturbances on limited-area domains. *Mon. Wea. Rev*., **123**, 1476–1504.

Nastrom GD, Eaton FD. 2006. Quasi-monochromatic inertia-gravity waves in the lower stratosphere from MST radar observations. *J. Geophys. Res.* **111**: D19103.

O'Sullivan, D., and T. J. Dunkerton, 1995: Generation of inertia-gravity waves in a simulated life cycle of baroclinic instability. *J. Atmos. Sci.,* **52**, 3695–3716.

Plougonven, R., and H. Teitelbaum, 2003: Comparison of a large-scale inertia–gravity wave as seen in the ECMWF analyses and from radiosondes. *Geophys. Res. Lett.,* **30,** 1954, doi:10.1029/2003GL017716.

Plougonven, R. and F. Zhang, 2007: On the forcing of inertia-gravity waves by synoptic-scale flows. *J. of the Atmos. Sci.,* **64**, 1737-1742.

Plougonven, R., and C. Snyder, 2007: Inertia-gravity waves spontaneously generated fronts. Part I: Different baroclinic life cycles. *J. Atmos. Sci.* **64**, 2502-2520.

Ratnam M.V., Tsuda T, Jacobi C, Aoyama Y (2004) Enhancement of gravity wave activity observed during a major southern hemisphere stratospheric warming by CHAMP/GPS measurements. Geophys Res Lett 31 (L16101), doi: 10.1029/2004GL019789

Reisner, J., R. J. Rasmussen, and R. T. Bruintjes, 1998: Explicit forecasting of supercooled liquid water in winter stoRMS using the MM5 Mesoscale Model. *Quart. J. Roy. Meteor. Soc*., **124B**, 1071–1107.

Sato, K., T. Kumakura and M. Takahashi, 1999: Gravity waves appearing in a high-

resolution GCM simulation. *J. Atmos. Sci.* **56**: 1005–1018.

Sato, K., 1994: A statistical study of the structure, saturation and sources of inertio-gravity waves in the lower stratosphere observed with the MU radar, *J. Atmos. Terr. Phys.,* **56**, 755–774.

Snyder, C., W. C. Skamarock, and R. Rotunno, 1993: Frontal dynamics near and following frontal collapse. *J. Atmos. Sci.,* **50,** 3194–3212.

Snyder, C., D. J. Muraki, R. Plougonven, and F. Zhang, 2007: Intertia-gravity waves Generated within a dipole vortex. *J. Atmos. Sci.*, **64**, 4417-4431.

Tsuda, T., M. Nishida, and C. Rocken, 2000: A global morphology of gravity wave activity in the stratosphere revealed by the GPS occultation data (GPS/MET), *J. Geophys. Res.*, **105**, 7257–7274.

Uccellini, L. W., and S. E. Koch, 1987: The synoptic setting and possible source mechanisms for mesoscale gravity wave events. *Mon. Wea. Rev*., **115**, 721–729.

Vaughan G. and R. M. Worthington, 2007: Inertia-gravity waves observed by the UK MST radar. *Quart. J. Roy. Meteor. Soc.*, **133**:179-188.

Wang, L., and M. A. Geller, 2003: Morphology of gravity wave energy as observed from four years (1998–2001) of high vertical resolution U.S. radiosonde data. *J. Geophys. Res.,* **108,** 4489-4496

Wang L., Wang, M.A. Geller and M.J. Alexander, 2005: Spatial and temporal variations of gravity wave parameters. Part I: Intrinsic frequency, wavelength, and vertical propagation direction, *J.Atmos. Sci.* **62** , 125–142.

Wang, S. and F. Zhang, 2007: Sensitivity of mesoscale gravity waves to the

baroclinicity of jet-front systems. *Monthly Weather Review*, **135**, 670-688.

Wang, S., F. Zhang, and C. Snyder, 2008: Generation and Propagation of Inertial Gravity Waves from Vortex Dipoles and Jets. *J. Atmos. Sci.*, submitted.

Wu, D. L., and J. W. Waters, 1996: Satellite observations of atmospheric variances: A possible indication of gravity waves, *Geophys. Res. Lett*., **23**, 3631–3634.

Wu, D. L., 2004: Mesoscale gravity wave variances from AMSU-A radiances, *Geophys. Res. Lett.* , **31**, L12114, doi:10.1029/ 2004GL019562.

Wu, D. L., and F. Zhang , 2004: A study of mesoscale gravity waves over North Atlantic with satellite observations and a mesoscale model. *J. Geophys. Res*., **109**, D22104., doi: 10.1029/2004JD005090.

Zhang, F., S. E. Koch, C. A. Davis, and M. L. Kaplan, 2001: Wavelet analysis and the governing dynamics of a large-amplitude gravity wave event along the east coast of the United States. *Quart. J. Roy. Meteor. Soc*., **127**, 2209-2245.

Zhang, F., S. E. Koch, and M. L. Kaplan, 2003: Numerical simulations of a large-amplitude gravity wave event. *Meteorology and Atmospheric Physics,*, **84**, 199-216

Zhang, F., 2004: Generation of mesoscale gravity waves in the upper-tropospheric jet-front systems. *J. Atmos. Sci.*, **61**, 440-457, 2004.

APPENDIX A

BRIEF INTRODUCTION TO THE REAL-TIME ASSIMILATION/FORECAST SYSTEM

This ensemble-based assimilation/forecast system (Fig. 14) assimilates radiosonde observations at every 00Z and 12Z, and then a 72-h ensemble forecast and a high-resolution gravity-wave forecast are made at 00Z with 45-km and 15-km resolution, respectively. Ensemble Kalman Filter (EnKF) with 30 members is applied on the weather research and forecasting (WRF) model (Zhang et al. 2006, Meng and Zhang 2007, 2008), which covers the whole U.S. continent and has 60 vertical levels up to 10 mb. The prior analyses are provided by previous ensembles, and the posterior EnKF analyses are used to initialize all START08 daily forecasts, where significant improvements are obtained from the flow-dependent EnKF assimilation process of radiosonde observations (refer to Fig. 15 as an example), therefore more forecast skills are expected due to the benefits of better model inputs for WRF model. On the other hand, a high-resolution operational forecast is archived for gravity wave applications, which is a unique tool to predict the potential mesoscale perturbations for the flight track designs.

Currently, this system is operated by Texas A&M University on a cluster platform supported by START08 program. With 32 free CPUs, each run (including data assimilation and all 72-h forecasts) costs about eight hours, and all of the forecasting products could be available at 14Z (8am MDT) for everyday uses of START08. About 40 gigabyte storage space is needed for one run, containing observation/analysis inputs and

model outputs, and they are archived on local hard disks for both prior-flight forecast and post-flight research uses. The daily forecast maps are placed on the START08 webpage (http://catalog.eol.ucar.edu/cgi-bin/start08/model/index).

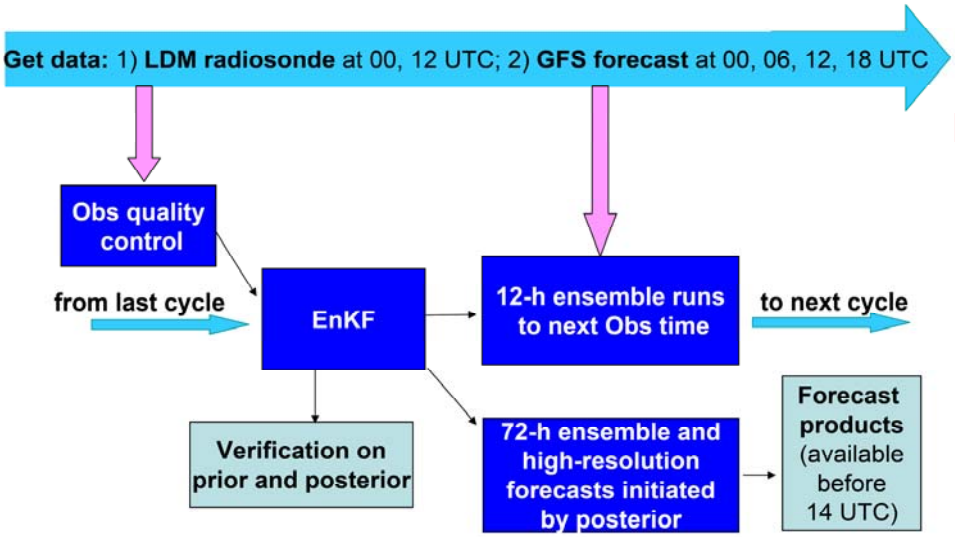

Fig.14 Flowchart of the real-time assimilation/forecast system for START08.

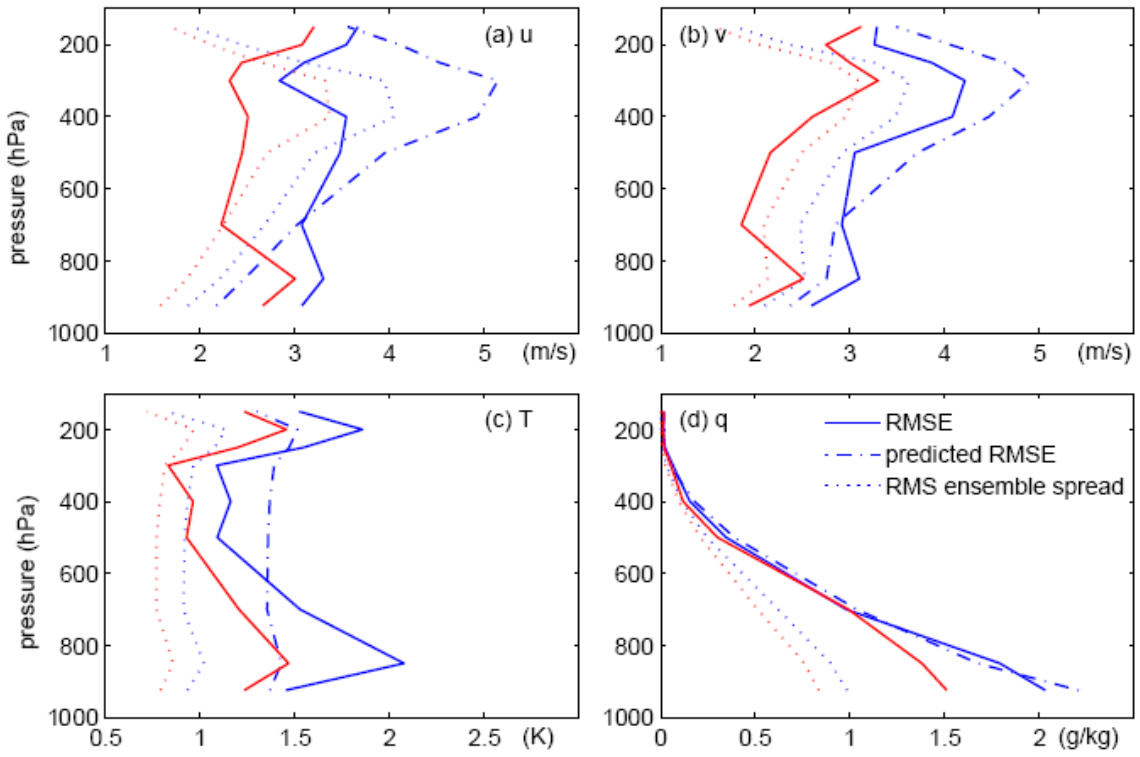

Fig.15 The RMS errors of EnKF prior (solid blue) and posterior analysis (solid red) against radiosonde oberservations, valid at 12Z 21 April 2008, for zonal wind (a), meridional wind (b), temperature (c) and mixing ratio (d). And predicted RMS error (RMS error plus observational error) (dashed dot) and ensemble spread (dot) are also shown for them.

VITA

Name: Meng Zhang

Address: Department of Atmospheric Sciences
Texas A&M University
College Station, TX 77843-3150

Email Address: mzhang@tamu.edu

Education: B.S., Atmospheric Sciences, Nanjing University, 2003
M.S., Meteorology, Nanjing University, 2006